XVIII International Conference on Water Resources
CMWR 2010
J. Carrera (Ed)

FINITE VOLUMES FOR THE SIMULATION OF UNSTEADY SHALLOW WATER FLOWS

P. Garcia-Navarro*, J. Murillo†

*Universidad de Zaragoza
Maria de Luna 3, 50018 Zaragoza, Spain
e-mail: pigar@unizar.es, web page: http://ghc.unizar.es

†Universidad de Zaragoza
Maria de Luna 3, 50018 Zaragoza, Spain
e-mail: Javier.Murillo@unizar.es, web page: http://ghc.unizar.es

Key words: Advanced numerical methods, water resources, model predictions

Summary. When applying the unsteady shallow water model to the simulation of overland flow in urban flooding problems it is necessary to handle correctly all kind of situations related to the complex geometry that can appear. The numerical model used to solve the system of equations has to provide well balanced solutions (equilibrium in cases of still water) and to maintain non-negative water depths for simulations involving wetting and drying transitions. Due to the complex topographic features involved in some cases, strong discontinuities in the bed elevation may appear, and as a result the suitability of the numerical model employed can be compromised. Godunov methods have been found a reliable tool to simulate realistic scenarios but, to ensure a correct performance of the numerical solution in all cases, the approximations involved to generate the numerical method have to be revisited. This revision results in new approximate solutions and a complete definition of the stability region avoiding additional tuning parameters commonly found in literature. Also, the proposed new solver indicates that the definition of well-balanced equilibrium in trivial cases is not sufficient to provide correct results: it is necessary to provide discrete evaluations of the source term that ensure energy dissipating solutions when demanded.

1 INTRODUCTION

There is a wide range of physical situations, such as flow in open channels and rivers, tsunami and flood modeling, that can be mathematically represented by first-order nonlinear systems of partial differential equations, whose derivation involves an assumption of the shallow water type. The system of equations in realistic shallow water models includes advective as well as source terms.

For sometime it has been accepted that the discretization of source terms can be as challenging as that of the non-linear advection terms. It must be said that for most cases, even naive discretizations of the source terms work reasonably well, but there are some well documented situations in which only sophisticated schemes can perform adequately. When solving real problems one is likely to encounter all sorts of situations, with a high probability that naive schemes will compromise the quality and reliability of the solution.

When incorporating the presence of the source terms in a given specific finite volume scheme (Roe's scheme is used here) the main focus has been traditionally put on how the numerical scheme can be modified so that it maintains a discrete balance between flux and source terms. In the context of the discretization of hyperbolic systems of conservation laws a fundamental point has been to get schemes that satisfy the preservation of steady-states such as still water equilibrium in the context of the shallow water system. The difficulty to build such schemes was pointed out by several authors and led to the notion of well-balanced schemes [20, 9, 19].

In this framework the development of robust and efficient explicit finite volume models of shallow water flow has been the matter of recent research in the computational hydraulics literature. A few efforts have been reported on the search for the best methods able to preserve the exact conservation property (C-property) [20] in presence of flow over irregular geometries [4, 11]. When dealing with simulation problems that involve bed variations and transient flow over a dry bed, these flow features impose a heavier restriction than the classical Courant-Friedrichs-Lewy (CFL) condition [6, 9, 19] on the time step size that may lead to inefficient computations. It is possible to avoid the necessity of reducing the time step and, at the same time, preventing instability and ensuring conservation at all times by a suitable flux difference redistribution [11, 13].

It can also be argued that the presence of source terms is the reason for the construction of new weak solutions appropriate to the nature of the equations, rather than the use of those constructed for the simple, homogeneous case. Even ensuring the discrete equilibrium formulated in well-balanced schemes, the direct application of the conclusions derived for the homogeneous case to cases with source terms leads to important difficulties. One of the most dramatic is the appearance of negative values of water depth, not only in wet/dry fronts, but also in initially wet/wet Riemann problems.

Gravity and friction are the main forces driving open channel flows. When using the shallow water model in hydraulic simulation, these forces participate in the dynamic equation as sources/sinks of momentum. In cases of steady shallow water flow with non-zero velocity, the discrete balance must be revisited [12].

George [7] presented a well balanced augmented approximate Riemann solver for the extended one dimensional shallow water equations including in the original solution vector two new variables: momentum flux and bottom surface. The solver is well-balanced and maintains a large class of steady states by the use of a properly defined steady state wave: a stationary jump discontinuity in the Riemann solution that acts as a source term. The idea of a stationary jump discontinuity is adapted to the method proposed

in this work where the original system is not enlarged. without modifying the original solution vector of conserved quantities (mass and momentum), we present augmented approximate Riemann solvers for the shallow water equations in the presence of a variable bottom surface and friction. They belong to the class of simple approximate solvers that use a set of propagating jump discontinuities, or waves, to approximate the true Riemann solution. Typically, a simple solver for a system of m conservation laws uses m such discontinuities. We present a three wave solver for the 1D shallow water equations system (two equations) and a four wave solver for the 2D case (three equations). In this work we go back to the original ideas of Roe using the upwind discretization of the source terms proposed by [20].

2 1D SYSTEMS OF CONSERVATION LAWS

A hyperbolic nonlinear systems of equations without source terms in 1D, can be expressed in integral form in terms of the conserved variable $\mathbf{U}$ and the flux $\mathbf{F}$ as:

$$\frac{\partial}{\partial t}\int_{x_1}^{x_2} \mathbf{U}dx + \mathbf{F}|_{x_2} - \mathbf{F}|_{x1} = 0 \tag{1}$$

where x_1, x_2 are the limits of a generic control volume. The differential formulation is obtained assuming smooth variation of the variables and an infinitesimal width of the control volume:

$$\frac{\partial \mathbf{U}}{\partial t} + \frac{\partial \mathbf{F}}{\partial x} = 0 \tag{2}$$

and from this formulation it is possible to define a Jacobian matrix $\mathbf{J}$

$$\mathbf{J} = \frac{d\mathbf{F}}{d\mathbf{U}} \tag{3}$$

Assuming that (1) is strictly hyperbolic with two real eigenvalues λ^1, λ^2 and eigenvectors $\mathbf{e}^1, \mathbf{e}^2$, it is possible define two matrices $\mathbf{P} = (\mathbf{e}^1, \mathbf{e}^2)$ and $\mathbf{P}^{-1}$ with the property that they diagonalize the Jacobian $\mathbf{J}$

$$\mathbf{J} = \mathbf{P}\mathbf{\Lambda}\mathbf{P}^{-1} \tag{4}$$

This means that the solution of a given a Riemann problem for (2) with initial values $\mathbf{U}_L, \mathbf{U}_R$, is a similarity solution. Figure 2 depicts the classical Riemann problem for a typical 2x2 homogeneous non-linear system, for which it is assumed that the left wave is a rarefaction and the right wave is a shock. The top frame shows the initial condition for a single component U_i of the vector of unknowns $\mathbf{U}$. The bottom frame of Figure 2 depicts the structure of the corresponding solution in the $x - t$ plane; characteristic curves are straight lines.

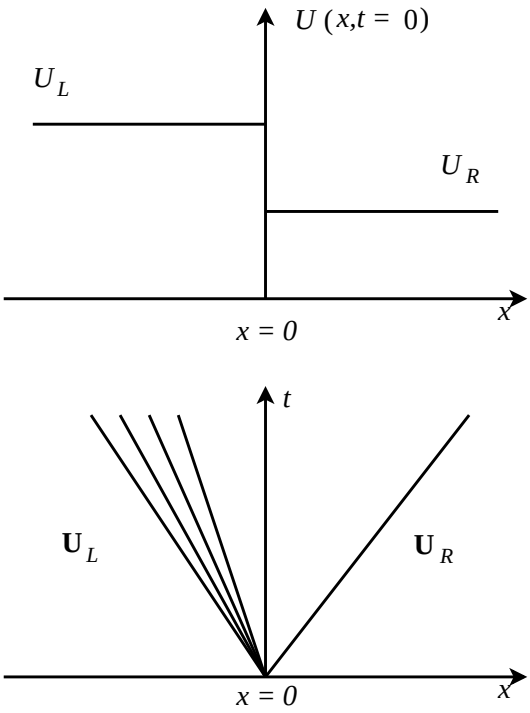

Figure 1: The classical Riemann problem for a typical 2x2 non-linear homogeneous system. Top frame: initial condition at $t = 0$ for a single component U of the vector of unknowns $\mathbf{U}$. Bottom frame: structure of the solution in the $x - t$ plane.

Figure 2 top depicts the structure of the solution solution after a time Δt. The solution has evolved in space according to the position of the rays that define the solution. In $x = 0$ the solution is constant for any value of t.

In order to obtain a numerical solution of system (2) we divide the domain in computational cells of constant size Δx: the i-th cell is defined by $[x_{i-1/2}, x_{i+1/2}]$ where $x_{i+1/2} = i\Delta x$ and the position of the center of the cell x_i is defined by $(i - 1/2)\Delta x$. Let Δt be the time step and $t^n = n\Delta t$ a generic time; assuming the usual notation we indicate with $\mathbf{U}_i^n$ the cell-average value of the solution $\mathbf{U}(x, t)$ for the ith cell at time t^n:

$$\mathbf{U}_i^n = \frac{1}{\Delta x} \int_{x_{i-1/2}}^{x_{i+1/2}} \mathbf{U}(x, t^n) dx. \tag{5}$$

$\mathbf{U}_i^n$ is therefore a piecewise constant approximation of the solution at time t^n,

To introduce the finite volume scheme, (2) is integrated in a volume or grid cell Ω that corresponds to an interval Δx in 1D :

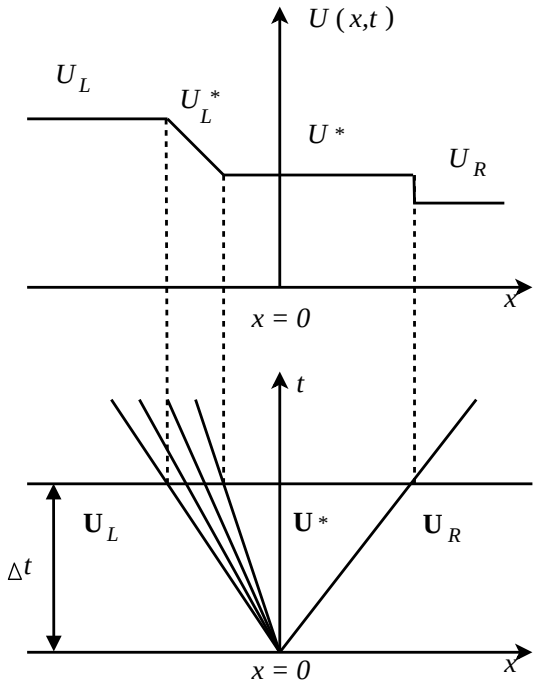

Figure 2: The classical Riemann problem for a typical 2x2 non-linear homogeneous system. Top frame: solution at $t = \Delta t$ for a single component U of the vector of unknowns $\mathbf{U}$. Bottom frame: structure of the solution in the $x - t$ plane.

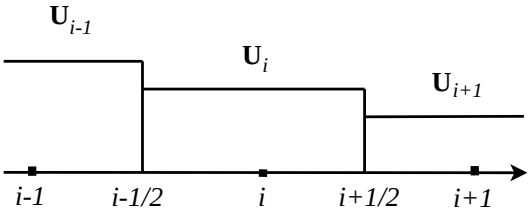

Figure 3: Piecewise constant approximation of the solution $\mathbf{U}_i^n$ at time t^n.

$$\frac{\partial}{\partial t}\int_\Omega \mathbf{U} d\Omega + \int_\Omega (\overrightarrow{\nabla}\mathbf{F}) d\Omega = 0 \tag{6}$$

and applying the Gauss theorem becomes

$$\frac{\partial}{\partial t}\int_\Omega \mathbf{U} d\Omega + \oint_{\partial\Omega} \mathbf{F}\mathbf{n} dl = 0 \tag{7}$$

where $\mathbf{n}$ is the outward unit normal vector to the volume Ω, that in the 1D approach leads to the following formulation:

$$\mathbf{U}_i^{n+1} = \mathbf{U}_i^n - \frac{\Delta t}{\Delta x}\left(\mathbf{F}^*_{i+1/2} - \mathbf{F}^*_{i-1/2}\right) \tag{8}$$

where $\mathbf{F}^*_{i+1/2}$ is a suitable numerical flux defined in the cell edge or node $i+1/2$, as shown in Figure 2.

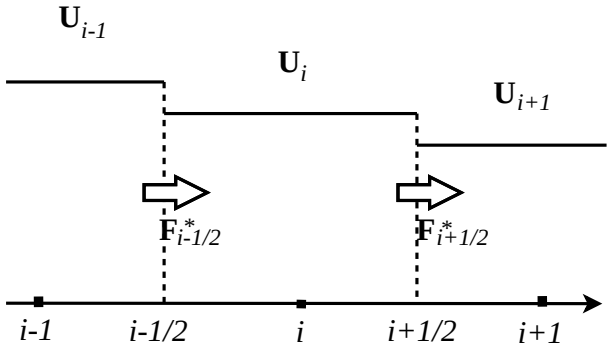

Figure 4: Contour integration domain of grid cell i .

For a nonlinear system of equations as (2) it is very important that the method be in conservative form, in order to ensure that weak solutions of the system of conservation laws are properly approximated. Recall that this form is derived directly from the integral form of the conservation laws in (1), wich is the correct equation to model when the solution is discontinous (as in shocks).

In the Godunov method the quantity $\mathbf{F}^*_{i+1/2}$ is determined by

$$\mathbf{F}^*_{i+1/2} = \mathbf{F}\left(\mathbf{U}^*_{i+1/2}\right) \tag{9}$$

where $\mathbf{U}^*_{i+1/2}$ is found by solving the Riemann Problem (RP) between states $\mathbf{U}_i$ and $\mathbf{U}_{i+1}$. The value $\mathbf{U}^*_{i+1/2}$ at $x = x_{i+1/2}$ in this Riemann solution is constant as the Riemann solution is a similarity solution. Then (8) can be expressed as

$$\mathbf{U}_i^{n+1} = \mathbf{U}_i^n - \frac{\Delta t}{\Delta x}\left(\mathbf{F}\left(\mathbf{U}^*_{i+1/2}\right) - \mathbf{F}\left(\mathbf{U}^*_{i-1/2}\right)\right) \tag{10}$$

as shown in Figure 2.

The first order Godunov method, provides a way to update the piecewise uniform quantities one time-step in the following way: the piecewise approximations (5), are considered as initial values of local RPs. The RP solutions are evolved for one time step; the resulting solution is cell-averaged again obtaining the piecewise solution at the new time

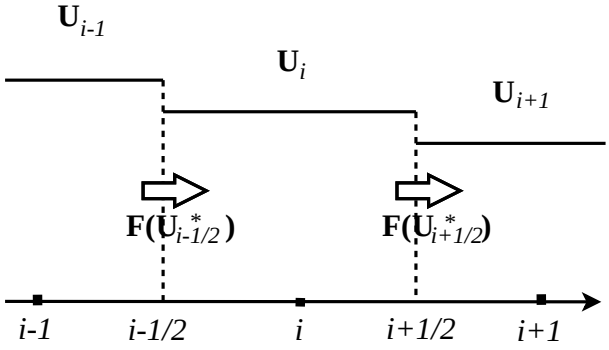

Figure 5: Contour integration domain of grid cell i .

level t^{n+1}.

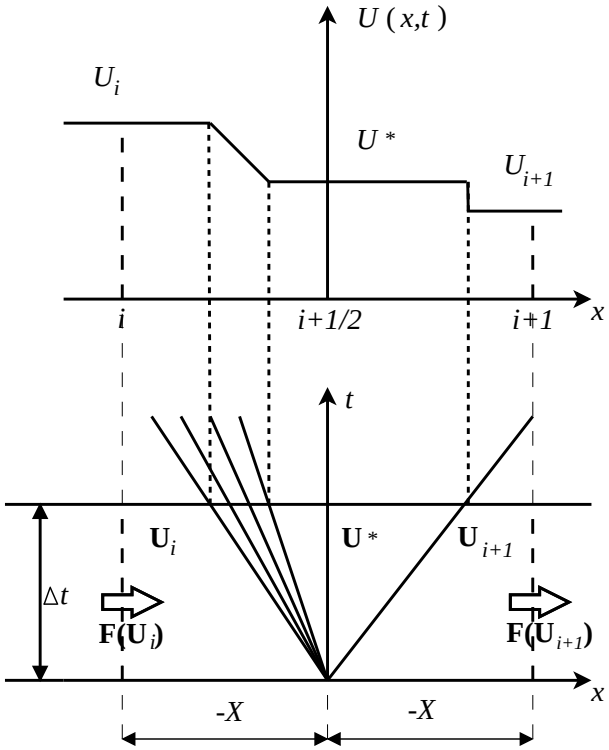

Figure 6: Top frame: solution at $t = \Delta t$ for a single component U of the vector of unknowns $\mathbf{U}$. Bottom frame: structure of the solution in the $x - t$ plane.

The evolution of the solution $\mathbf{U}(x, t)$ at every local RP can be also analysed considering a new control volume defined by a time interval $[0, \Delta t]$ and a space interval $[-X, X]$,

where

$$-X \leq \lambda_{min}\Delta t, \quad X \geq \lambda_{max}\Delta t \tag{11}$$

being $\lambda_{min}\Delta t, \lambda_{max}\Delta t$ the positions of the slowest and the fastest wave at $t = \Delta t$. The initial volume at time $t = 0$ given by $X\left(\mathbf{U}_{i+1} + \mathbf{U}_i\right)$ changes due to the action of fluxes $\mathbf{F}(\mathbf{U}_{i+1})$ and $\mathbf{F}(\mathbf{U}_i)$ in time. The local RP is defined by

$$\begin{gathered} \frac{\partial \mathbf{U}}{\partial t} + \frac{\partial \mathbf{F}}{\partial x} = 0 \\ \mathbf{U}(x,0) = \begin{cases} \mathbf{U}_i & if \quad x < 0 \\ \mathbf{U}_{i+1} & if \quad x > 0 \end{cases} \end{gathered} \tag{12}$$

Integrating (12) over the control volume $[-X, X] \times [0, \Delta t]$,where X satisfies (11) we obtain

$$\int_{x=-X}^{x=+X} \int_{t=0}^{t=\Delta t} \left(\frac{\partial \mathbf{U}}{\partial t} + \frac{\partial \mathbf{F}}{\partial x} \right) \, dxdt = 0 \tag{13}$$

or

$$\int_{-X}^{+X} \left[\mathbf{U}(x,\Delta t) - \mathbf{U}(x,0)\right] dx + \int_{0}^{\Delta t} \left(\mathbf{F}(\mathbf{U}_{i+1}) - \mathbf{F}(\mathbf{U}_i)\right) dt = 0 \tag{14}$$

that can also be written

$$\int_{-X}^{+X} \mathbf{U}(x,\Delta t)dx - X\left(\mathbf{U}_{i+1} + \mathbf{U}_i\right) + \left(\mathbf{F}(\mathbf{U}_{i+1}) - \mathbf{F}(\mathbf{U}_i)\right) \, \Delta t = 0 \tag{15}$$

The solution $\mathbf{U}$ at time $t = \Delta t$, $\mathbf{U}(x, \Delta t)$, satisfies therefore the following property:

$$\int_{-X}^{+X} \mathbf{U}(x,\Delta t) \, dx = X\left(\mathbf{U}_{i+1} + \mathbf{U}_i\right) - \left(\mathbf{F}(\mathbf{U}_{i+1}) - \mathbf{F}(\mathbf{U}_i)\right)\Delta t \tag{16}$$

This property provides a condition over the exact solution, although the exact solution is not described yet. The Godunov method provides the way to update the solution but does not provide an exact solution for any general RP in any system of equations. In certain cases, it is possible to reconstruct the exact solution $\mathbf{U}(x,t)$ but its computation is extremily expensive and in most cases impossible. Another alternative is to use an approximate solution of $\mathbf{U}(x,t)$, that we will referred to as $\hat{\mathbf{U}}(x,t)$.

2.1 Approximate solution of the Riemann problem

In the Roe approach, the solution of each RP is obtained from the exact solution of a locally linearized problem (ARP). This solution must fulfill the so called Consistency Condition, i.e. that the integral of the solution $\hat{\mathbf{U}}(x,t)$ of the ARP over a suitable control volume must be equal to the integral of the exact solution of (12) over the same control volume:

$$\int_{-X}^{+X} \hat{\mathbf{U}}(x,\Delta t)\, dx = \int_{-X}^{+X} \mathbf{U}(x,\Delta t)\, dx \tag{17}$$

or:

$$\int_{-X}^{+X} \hat{\mathbf{U}}(x,\Delta t)\, dx = X\left(\mathbf{U}_{i+1}+\mathbf{U}_i\right) - \left(\mathbf{F}(\mathbf{U}_{i+1}) - \mathbf{F}(\mathbf{U}_i)\right)\Delta t \tag{18}$$

In the Roe formulation, RP (12) is approximated by using the following linear ARP:

$$\begin{gathered} \frac{\partial \hat{\mathbf{U}}}{\partial t} + \mathbf{J}^* \frac{\partial \hat{\mathbf{U}}}{\partial x} = 0 \\ \hat{\mathbf{U}}(x,0) = \begin{cases} \mathbf{U}_i & if \quad x<0 \\ \mathbf{U}_{i+1} & if \quad x>0 \end{cases} \end{gathered} \tag{19}$$

where $\mathbf{J}^*(\mathbf{U}_i, \mathbf{U}_{i+1})$ is a constant matrix. Integrating (52) over the control volume $[-X, X]\times [0, \Delta t]$,where X satisfies (11):

$$\int_{x=-X}^{x=+X} \int_{t=0}^{t=\Delta t} \left(\frac{\partial \hat{\mathbf{U}}}{\partial t} + \mathbf{J}^* \frac{\partial \hat{\mathbf{U}}}{\partial x} \right) dxdt = 0 \tag{20}$$

or

$$\int_{x=-X}^{x=+X} \hat{\mathbf{U}}(x,1)dx - X\left(\mathbf{U}_{i+1}+\mathbf{U}_i\right) + \mathbf{J}^*\left(\mathbf{U}_{i+1}-\mathbf{U}_i\right)\ \Delta t = 0 \tag{21}$$

Then, the solution $\hat{\mathbf{U}}$ at time $t=\Delta t$, $\hat{\mathbf{U}}(x,\Delta t)$, satisfies the following property:

$$\int_{-X}^{+X} \hat{\mathbf{U}}(x,1)\, dx = X\left(\mathbf{U}_{i+1}+\mathbf{U}_i\right) - \mathbf{J}^*(\mathbf{U}_i,\mathbf{U}_{i+1})\left(\mathbf{U}_{i+1}-\mathbf{U}_i\right)\Delta t \tag{22}$$

Since we want to satisfy (50), the constraint that follows is:

$$\delta\mathbf{F} = \mathbf{J}^*_{i+1/2}\delta\mathbf{U}_{i+1/2} \tag{23}$$

with $\delta\mathbf{F}_{i+1/2} = \mathbf{F}(\mathbf{U}_{i+1}) - \mathbf{F}(\mathbf{U}_i)$ and $\delta\mathbf{U}_{i+1/2} = \mathbf{U}_{i+1} - \mathbf{U}_i$ Moreover, two more conditions are standard requirements for the Roe method.

$$\begin{gathered} \mathbf{J}^*_{i+1/2}(\mathbf{U}_{i+1},\mathbf{U}_i) \quad \text{is diagonalizable with real eigenvalues} \\ \mathbf{J}^*_{i+1/2}(\mathbf{U}_{i+1},\mathbf{U}_i) \rightarrow \mathbf{J}^*_{i+1/2}(\mathbf{U}_i) \quad \text{smoothly } as\ \mathbf{U}_{i+1}\rightarrow\mathbf{U}_i \end{gathered} \tag{24}$$

Considering that it is possible to define an approximate Jacobian $\tilde{\mathbf{J}}_{i+1/2}$, characterized by a set of approximate eigenvalues $\widetilde{\lambda}^1, \widetilde{\lambda}^2$ and eigenvectors $\widetilde{\mathbf{e}}^1, \widetilde{\mathbf{e}}^2$, two approximate matrices, $\widetilde{\mathbf{P}} = (\widetilde{\mathbf{e}}^1, \widetilde{\mathbf{e}}^2)$ and $\widetilde{\mathbf{P}}^{-1}$ are built with the following property:

$$\widetilde{\mathbf{J}}_{i+1/2} = \widetilde{\mathbf{P}}_{i+1/2}\widetilde{\mathbf{\Lambda}}_{i+1/2}\widetilde{\mathbf{P}}^{-1}_{i+1/2} \tag{25}$$

The difference in vector $\mathbf{U}$ across the grid edge is projected onto the matrix eigenvectors basis:

$$\delta \mathbf{U}_{i+1/2} = \widetilde{\mathbf{P}}_{i+1/2} \mathbf{A}_{i+1/2} \tag{26}$$

with $\mathbf{A}_{i+1/2} = (\alpha^1, \alpha^2)^T_{i+1/2}$. Expressing all terms more compactly:

$$\delta \mathbf{F}_{i+1/2} = \sum_{m=1}^{N_\lambda} \left(\widetilde{\lambda} \alpha \widetilde{\mathbf{e}} \right)^m_{i+1/2} \tag{27}$$

so that the desired matrix in (53) is

$$\mathbf{J}^*_{i+1/2} = (\widetilde{\mathbf{P}} \widetilde{\mathbf{\Lambda}}^* \widetilde{\mathbf{P}}^{-1})_{i+1/2} \tag{28}$$

where $\widetilde{\mathbf{\Lambda}}_{i+1/2}$ is a diagonal matrix with eigenvalues $\widetilde{\lambda}^m_{i+1/2}$ in the main diagonal:

$$\widetilde{\mathbf{\Lambda}}_{i+1/2} = \begin{pmatrix} \widetilde{\lambda}^1 & 0 \\ 0 & \widetilde{\lambda}^2 \end{pmatrix}_{i+1/2} \tag{29}$$

2.2 Application to the 1D shallow water equations

For the 1D shallow water equations the relevant integral formulation in (1) derives from the depth-averaged equations of mass conservation and of momentum, with

$$\mathbf{U} = \begin{pmatrix} h \\ hu \end{pmatrix} \quad \mathbf{F} = \begin{pmatrix} hu \\ hu^2 + \frac{1}{2} g h^2 \end{pmatrix} \tag{30}$$

where h represents the water depth, u the depth averaged component of the velocity vector and g is the acceleration of the gravity. The above formulation is written in terms of the unit discharge and not valid for arbitrary cross sections. In order to extend the following discussion to general 1D problems [5] should be followed.

The Jacobian leads to two real eigenvalues λ^1, λ^2 and eigenvectors $\mathbf{e}^1, \mathbf{e}^2$,

$$\begin{array}{cc} \lambda^1 = u - c & \lambda^2 = u + c \\ \mathbf{e}^1 = \begin{pmatrix} 1 \\ u - c \end{pmatrix} & \mathbf{e}^2 = \begin{pmatrix} 1 \\ u + c \end{pmatrix} \end{array} \tag{31}$$

with $c = \sqrt{gh}$.

The approximate Jacobian $\widetilde{\mathbf{J}}$ [14] is

$$\widetilde{\mathbf{J}}_{i+1/2} = \begin{pmatrix} 0 & 1 \\ \widetilde{c}^2 - \widetilde{u}^2 & 2\widetilde{u} \end{pmatrix}_{i+1/2} \qquad \delta \mathbf{F}_{i+1/2} = \widetilde{\mathbf{J}}_{i+1/2} \delta \mathbf{U}_{i+1/2} \tag{32}$$

with

$$\widetilde{c} = \sqrt{g\frac{h_i + h_{i+1}}{2}} \quad \widetilde{u} = \frac{u_{i+1}\sqrt{h_{i+1}} + u_i\sqrt{h_i}}{\sqrt{h_{i+1}} + \sqrt{h_i}} \tag{33}$$

and the resulting sets of approximate eigenvalues and eigenvectors are

$$\begin{array}{cc} \widetilde{\lambda}^1 = \widetilde{u} - \widetilde{c} & \widetilde{\lambda}^2 = \widetilde{u} + \widetilde{c} \\ \widetilde{\mathbf{e}}^1 = \begin{pmatrix} 1 \\ \widetilde{u} - \widetilde{c} \end{pmatrix} & \widetilde{\mathbf{e}}^2 = \begin{pmatrix} 1 \\ \widetilde{u} + \widetilde{c} \end{pmatrix} \end{array} \tag{34}$$

2.2.1 Two wave approximate Riemann solution

The solution for $\hat{\mathbf{U}}(x,t)$ is governed by the celerities in $\widetilde{\mathbf{\Lambda}}_{i+1/2}$ and consists of three regions. Depending on the flow conditions, the approximate solution that satisfies (50) changes and the solution is given by

$$\hat{\mathbf{U}}(x,t) = \begin{cases} \mathbf{U}_i^n & \text{if} \quad x - \widetilde{\lambda}^1 t < 0 \\ \mathbf{U}_{i+1/2} & \text{if} \quad x - \widetilde{\lambda}^1 t > 0 \text{ and } x - \widetilde{\lambda}^2 t < 0 \\ \mathbf{U}_{i+1}^n & \text{if} \quad x - \widetilde{\lambda}^2 t > 0 \end{cases} \tag{35}$$

with

$$\begin{array}{c} \mathbf{U}_{i+1/2}(\mathbf{U}_{i+1}, \mathbf{U}_i) = \mathbf{U}_i^n + (\alpha\widetilde{\mathbf{e}})_{i+1/2}^1 \\ \mathbf{U}_{i+1/2}(\mathbf{U}_{i+1}, \mathbf{U}_i) = \mathbf{U}_{i+1}^n - (\alpha\widetilde{\mathbf{e}})_{i+1/2}^2 \end{array} \tag{36}$$

According to this solution in the subcritical case, Figure 2.2.1, the solution is given by $\mathbf{U}^* = \mathbf{U}_{i+1/2}$, in the supercritical case with $u > 0$, Figure 2.2.1, the solution is given by $\mathbf{U}^* = \mathbf{U}_i$ and in the supercritical case with $u < 0$, Figure 2.2.1, the solution is given by $\mathbf{U}^* = \mathbf{U}_{i+1}$

Following Godunov method these RP solutions are then evolved for a time equal to the time step, the resulting solution is cell-averaged obtaining the piecewise solution at the new time level t^{n+1}. If both i and $i+1$ are subcritical, the integral volume in cell $[0, \Delta x] \times [0, \Delta t]$ is depicted in Figure 11. Focusing on the updating rule for cell i:

$$\mathbf{U}_i^{n+1}\Delta x = \mathbf{U}_{i-1/2}(\widetilde{\lambda}_{i-1/2}^2\Delta t) + \mathbf{U}_i^n(\Delta x - \widetilde{\lambda}_{i-1/2}^2\Delta t + \widetilde{\lambda}_{i+1/2}^1\Delta t) + \mathbf{U}_{i+1/2}(-\widetilde{\lambda}_{i+1/2}^1\Delta t) \tag{37}$$

that can be rewritten as

$$\mathbf{U}_i^{n+1}\Delta x = \mathbf{U}_i^n(\Delta x) + (\mathbf{U}_{i-1/2} - \mathbf{U}_i^n)(\widetilde{\lambda}_{i-1/2}^2\Delta t) + (\mathbf{U}_i^n - \mathbf{U}_{i+1/2})(\widetilde{\lambda}_{i+1/2}^1\Delta t) \tag{38}$$

and considering (36) the updated value $\mathbf{U}_i^{n+1}$ is:

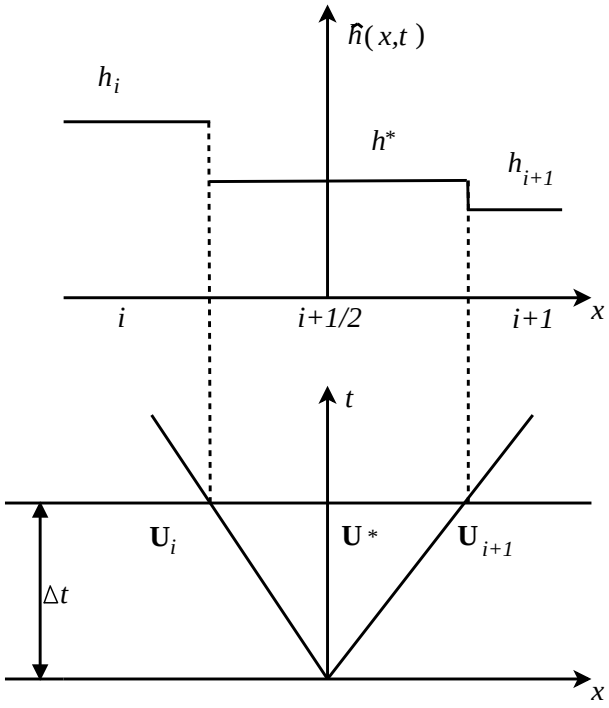

Figure 7: Top frame: approximate solution at $t = \Delta t$ for h. Bottom frame: structure of the approximate solution $\hat{\mathbf{U}}$ in the $x - t$ plane for the subcritical case.

$$\mathbf{U}_i^{n+1} = \mathbf{U}_i^n - (\alpha\tilde{\mathbf{e}}\tilde{\lambda})_{i-1/2}^2 \frac{\Delta t}{\Delta x} - (\alpha\tilde{\mathbf{e}}\tilde{\lambda})_{i+1/2}^1 \frac{\Delta t}{\Delta x} \tag{39}$$

In general Godunov's method can be formulatted by meas of the flux difference in each cell egde:

$$\mathbf{U}_i^{n+1} = \mathbf{U}_i^n - \left((\delta\mathbf{F})_{i-1/2}^+ + (\delta\mathbf{F})_{i+1/2}^- \right) \frac{\Delta t}{\Delta x} \tag{40}$$

where the fluxes in a general intercell edge $i + 1/2$ are computed as follows:

$$(\delta\mathbf{F})_{i+1/2}^{\pm} = \sum_{m=1}^{N_\lambda} \left(\tilde{\lambda}^{\pm} \alpha\tilde{\mathbf{e}} \right)_{i+1/2}^m \tag{41}$$

accounting only for the in-going waves to the domain, by means of the upwinding of the waves:

$$\tilde{\lambda}_{i+1/2}^{\pm,m} = \frac{1}{2}(\tilde{\lambda} \pm |\tilde{\lambda}|) \tag{42}$$

Straightforward algebraic manipulation converts (64) to an equivalent numerical flux-based finite volume scheme [8],

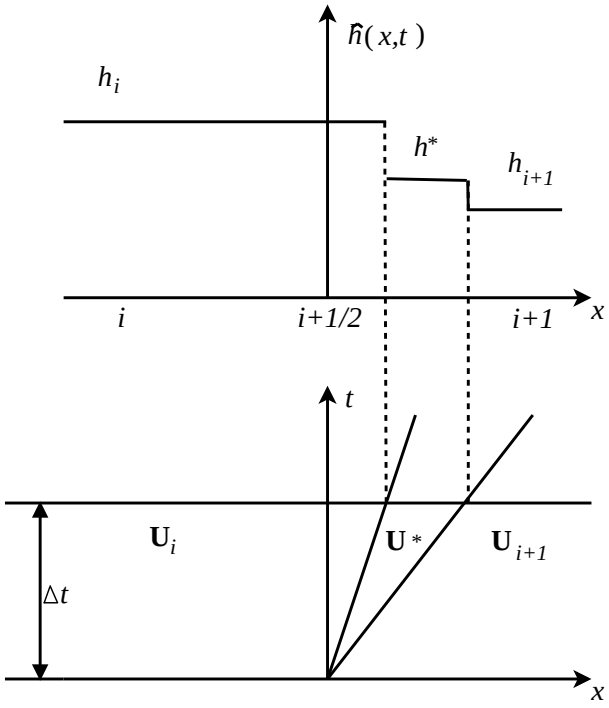

Figure 8: Top frame: approximate solution at $t = \Delta t$ for h. Bottom frame: structure of the approximate solution $\hat{\mathbf{U}}$ in the $x - t$ plane for the supercritical case,$u > 0$.

$$\mathbf{U}_i^{n+1} = \mathbf{U}_i^n - (\mathbf{F}^*_{i+1/2} - \mathbf{F}^*_{i-1/2})\frac{\Delta t}{\Delta x} \tag{43}$$

in which the numerical flux (denoted by an asterisk) for first-order upwinding is given by

$$\mathbf{F}^*_{i+1/2} = \frac{1}{2}(\mathbf{F}_{i+1} + \mathbf{F}_i) - \frac{1}{2}\left(\mathbf{P}|\widetilde{\mathbf{\Lambda}}|\mathbf{P}^{-1}\delta\mathbf{U}\right)_{i+1/2} \tag{44}$$

with a similar expression for $\mathbf{F}^*_{i-1/2}$.

In Figure 11 the time step is small enough so that there is no interaction of waves from neighboring Riemann problems. This would be necessary if we wanted to construct the solution at $\mathbf{U}_i^{n+1}$ in order to explicitly calculate the cell average (63). However, according to [9], in order to use the flux formula (65) it is only necessary that the edge values $\hat{\mathbf{U}}(x,t)$ remain constant in time over the entire time step, which allows a time step roughly twice as large and the time step is limited by

$$\Delta t \leq \Delta t^{\widetilde{\lambda}} \qquad \Delta t^{\widetilde{\lambda}} = \frac{\Delta x}{\max_{m=1,2}|\widetilde{\lambda}^m|} \tag{45}$$

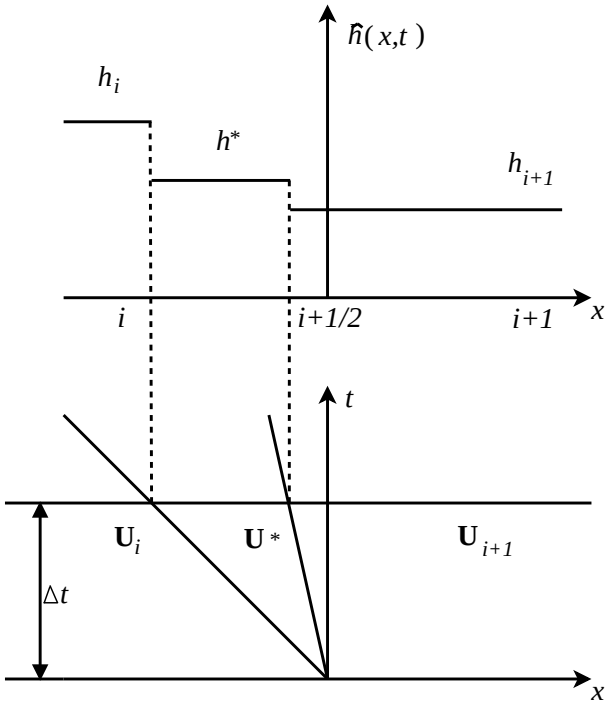

Figure 9: Top frame: approximate solution at $t = \Delta t$ for h. Bottom frame: structure of the approximate solution $\hat{\mathbf{U}}$ in the $x - t$ plane for the supercritical case,$u < 0$.

3 1D Systems of conservation laws with source terms

The discussion is next extended to hyperbolic nonlinear systems of equations with source terms in 1D, that expressed in integral form are:

$$\frac{\partial}{\partial t}\int_{x_1}^{x_2} \mathbf{U}dx + \mathbf{F}|_{x_2} - \mathbf{F}|_{x1} - \int_{x_1}^{x_2} \mathbf{S}dx = 0 \tag{46}$$

The differential formulation is obtained assuming smooth variation of the variables and an infinitesimal width of the control volume:

$$\frac{\partial \mathbf{U}}{\partial t} + \frac{\partial \mathbf{F}}{\partial x} = \mathbf{S} \tag{47}$$

In the case of systems of conservation laws with source terms we will assume that the solution of a given RP for (47) with initial values $\mathbf{U}_i, \mathbf{U}_{i+1}$

$$\begin{gathered} \frac{\partial \mathbf{U}}{\partial t} + \frac{\partial \mathbf{F}}{\partial x} = \mathbf{S} \\ \mathbf{U}(x,0) = \begin{cases} \mathbf{U}_i & if \quad x < 0 \\ \mathbf{U}_{i+1} & if \quad x > 0 \end{cases} \end{gathered} \tag{48}$$

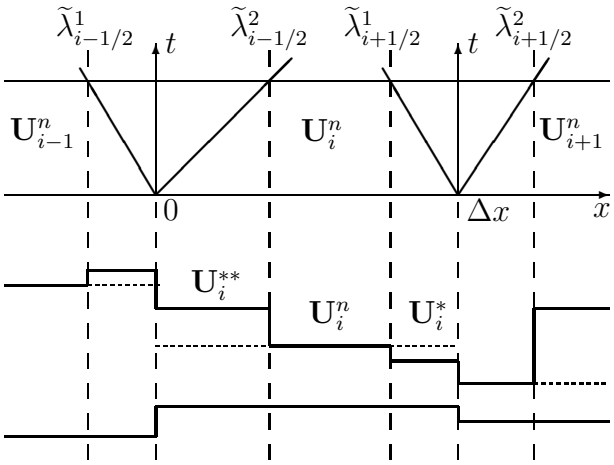

Figure 10: Control volume in the Godunov method

is also a similarity solution where the characteristic lines are also straight lines. Althought we do not known the wave estruture of the solution, it is possible to integrate (48)in a volume defined by a time interval $[0, \Delta t]$ and a space interval $[-X, X]$, defining X as in (11), also assuming that the solution is limited by the maximum and minimun of the homogenous part of the PDE in (48).

$$\int_{-X}^{+X} \mathbf{U}(x,1)\, dx = X\left(\mathbf{U}_{i+1} + \mathbf{U}_i\right) - \left(\mathbf{F}(\mathbf{U}_{i+1}) - \mathbf{F}(\mathbf{U}_i)\right)\Delta t + \int_0^{\Delta t}\int_{-X}^{+X} \mathbf{S}\, dx\, dt \qquad (49)$$

Since the source term is not necessarily constant in time, we assume the following time linearization of the Consistency Condition:

$$\int_{-X}^{+X} \hat{\mathbf{U}}(x,1)\, dx = X\left(\mathbf{U}_{i+1} + \mathbf{U}_i\right) - \left(\mathbf{F}(\mathbf{U}_{i+1}) - \mathbf{F}(\mathbf{U}_i)\Delta t - \mathbf{S}_{i+1/2}\right) \qquad (50)$$

where

$$\mathbf{S}_{i+1/2} = \int_{-X}^{+X} \mathbf{S}(x,0)\, dx \qquad (51)$$

is a suitable numerical source vector.

In this formulation, RP (12) is approximated by using the following linear ARP:

$$\frac{\partial \hat{\mathbf{U}}}{\partial t} + \mathbf{J}^* \frac{\partial \hat{\mathbf{U}}}{\partial x} = 0$$
$$\hat{\mathbf{U}}(x,0) = \begin{cases} \mathbf{U}_i & if \quad x < 0 \\ \mathbf{U}_{i+1} & if \quad x > 0 \end{cases} \tag{52}$$

where $\mathbf{J}^*(\mathbf{U}_i, \mathbf{U}_{i+1})$ is a constant matrix. Integrating (52) over the control volume $[-X, X] \times [0, \Delta t]$,where X satisfies (11):

$$\int_{-X}^{+X} \hat{\mathbf{U}}(x,1)\, dx = X\left(\mathbf{U}_{i+1} + \mathbf{U}_i\right) - \mathbf{J}^*(\mathbf{U}_i, \mathbf{U}_{i+1})\left(\mathbf{U}_{i+1} - \mathbf{U}_i\right)\Delta t \tag{53}$$

Since we want to satisfy (50), the constraint that follows is:

$$\delta \mathbf{F}_{i+1/2} - \mathbf{S}_{i+1/2} = \mathbf{J}^*_{i+1/2} \delta \mathbf{U}_{i+1/2} \tag{54}$$

The difference in vector $\mathbf{U}$ across the grid edge is projected onto the matrix eigenvectors basis and the same for the source term:

$$\delta \mathbf{U}_{i+1/2} = \widetilde{\mathbf{P}}_{i+1/2} \mathbf{A}_{i+1/2} \qquad \mathbf{S}_{i+1/2} = \widetilde{\mathbf{P}}_{i+1/2} \mathbf{B}_{i+1/2} \tag{55}$$

with $\mathbf{A}_{i+1/2} = (\alpha^1, \alpha^2)^T_{i+1/2}$ and $\mathbf{B}_{i+1/2} = (\beta^1, \beta^2)^T_{i+1/2}$. Expressing all terms more compactly:

$$\delta \mathbf{F}_{i+1/2} - \mathbf{S}_{i+1/2} = \sum_{m=1}^{N_\lambda} \left(\widetilde{\lambda}^* \alpha \widetilde{\mathbf{e}}\right)^m_{i+1/2} \tag{56}$$

where

$$\widetilde{\lambda}^{*,m}_{i+1/2} = \widetilde{\lambda}^m_{i+1/2}\, \theta^m_{i+1/2} \qquad \theta^m_{i+1/2} = \left(1 - \frac{\beta}{\widetilde{\lambda}\alpha}\right)^m_{i+1/2} \tag{57}$$

so that the desired matrix in (53) is

$$\mathbf{J}^*_{i+1/2} = (\widetilde{\mathbf{P}} \widetilde{\mathbf{\Lambda}}^* \widetilde{\mathbf{P}}^{-1})_{i+1/2} \tag{58}$$

with $\widetilde{\mathbf{\Lambda}}^* = \widetilde{\mathbf{\Lambda}} \mathbf{\Theta}$, where $\widetilde{\mathbf{\Lambda}}_{i+1/2}$ is a diagonal matrix with eigenvalues $\widetilde{\lambda}^m_{i+1/2}$ in the main diagonal:

$$\widetilde{\mathbf{\Lambda}}_{i+1/2} = \begin{pmatrix} \widetilde{\lambda}^1 & 0 \\ 0 & \widetilde{\lambda}^2 \end{pmatrix}_{i+1/2} \tag{59}$$

and $\mathbf{\Theta}_{i+1/2}$ is a diagonal matrix with $\theta^m_{i+1/2}$ in the main diagonal:

$$\Theta_{i+1/2} = \begin{pmatrix} \theta^1 & 0 \\ 0 & \theta^2 \end{pmatrix}_{i+1/2} \tag{60}$$

3.1 Application to the 1D shallow water equations with source terms

Including the relevant source terms in the 1D shallow water equations:

$$\mathbf{U} = \begin{pmatrix} h \\ hu \end{pmatrix} \quad \mathbf{F} = \begin{pmatrix} hu \\ hu^2 + \frac{1}{2}gh^2 \end{pmatrix} \qquad \mathbf{S} = \begin{pmatrix} 0 \\ \frac{p_b}{\rho_w} - \frac{\tau_b}{\rho_w} \end{pmatrix} \tag{61}$$

The source term of the system is split in two kind of terms. The terms p_b and τ_b are the pressure along the bottom and the shear stress in the x direction respectively, with ρ_w the density of water. The above formulation is written in terms of the unit discharge and not valid for arbitrary cross sections. In order to extend the following discussion to general 1D problems [5] should be followed.

Assuminf a hydrostatic pressure distribution, the following differential equation for the bottom slope can be obtained:

$$\frac{p_b}{\rho_w} = -gh\frac{\partial z}{\partial x} \tag{62}$$

3.1.1 A three wave approximate Riemann solution

Depending on the flow conditions, three approximate solutions that satisfy (50), are proposed. The solutions for $\hat{\mathbf{U}}(x,t)$ are governed by the celerities in $\widetilde{\mathbf{\Lambda}}_{i+1/2}$ and each one consists of four regions.

The details of the approximate Riemann solution for each case are provided in [**?**].

Following Godunov's method these RP solutions are then evolved for a time equal to the time step, the resulting solution is cell-averaged obtaining the piecewise solution at the new time level t^{n+1}. If both i and $i+1$ are subcritical, the integral volume in cell $[0,\Delta x]\times[0,\Delta t]$ is depicted in Figure 11. Focusing on the updating rule for cell i:

$$\mathbf{U}_i^{n+1}\Delta x = \mathbf{U}_i^{**}(\widetilde{\lambda}^2_{i-1/2}\Delta t) + \mathbf{U}_i^{n}(\Delta x - \widetilde{\lambda}^2_{i-1/2}\Delta t + \widetilde{\lambda}^1_{i+1/2}\Delta t) + \mathbf{U}_i^{*}(-\widetilde{\lambda}^1_{i+1/2}\Delta t) \tag{63}$$

that can be rewritten as

$$\mathbf{U}_i^{n+1}\Delta x = \mathbf{U}_i^{n}(\Delta x) + (\mathbf{U}_i^{**} - \mathbf{U}_i^{n})(\widetilde{\lambda}^2_{i-1/2}\Delta t) + (\mathbf{U}_i^{n} - \mathbf{U}_i^{*})(\widetilde{\lambda}^1_{i+1/2}\Delta t) \tag{64}$$

and considering (36) the updated value $\mathbf{U}_i^{n+1}$ is:

$$\mathbf{U}_i^{n+1} = \mathbf{U}_i^{n} - (\theta\alpha\tilde{\mathbf{e}}\widetilde{\lambda})^2_{i-1/2}\frac{\Delta t}{\Delta x} - (\theta\alpha\tilde{\mathbf{e}}\widetilde{\lambda})^1_{i+1/2}\frac{\Delta t}{\Delta x} \tag{65}$$

Straightforward algebraic manipulation converts (64) to an equivalent numerical flux-based finite volume scheme [8],

$$\mathbf{U}_i^{n+1} = \mathbf{U}_i^{n} - (\mathbf{F}^*_{i+1/2} - \mathbf{F}^*_{i-1/2})\frac{\Delta t}{\Delta x} + (\mathbf{S}^-_{i+1/2} + \mathbf{S}^+_{i-1/2})\frac{\Delta t}{\Delta x} \tag{66}$$

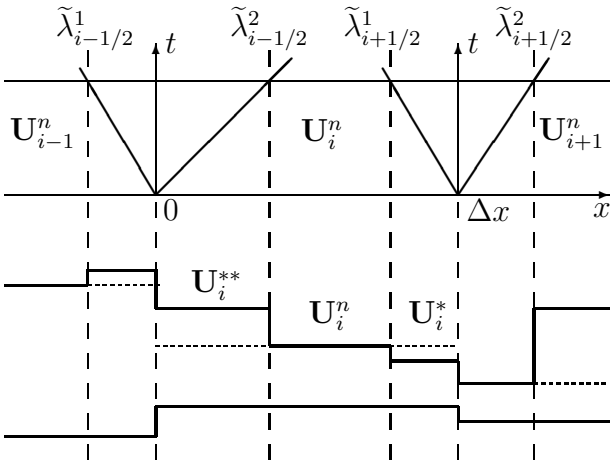

Figure 11: Control volume in the Godunov method

in which the numerical flux (denoted by an asterisk) for first-order upwinding is given by

$$\mathbf{F}^*_{i+1/2} = \frac{1}{2}(\mathbf{F}_{i+1} + \mathbf{F}_i) - \frac{1}{2}\left(\mathbf{P}|\widetilde{\mathbf{\Lambda}}|\mathbf{P}^{-1}\delta\mathbf{U}\right)_{i+1/2} \tag{67}$$

with a similar expression for $\mathbf{F}^*_{i-1/2}$ and

$$\mathbf{S}^{\pm}_{i+1/2} = \left(\mathbf{P}\mathbf{I}^{\pm}\mathbf{P}^{-1}\mathbf{S}\right)_{i+1/2} \tag{68}$$

and $\mathbf{I}^{\pm} = \mathbf{\Lambda}^{-1}\frac{1}{2}\left(\mathbf{\Lambda} \pm |\mathbf{\Lambda}|\right)$.

In Figure 11 the time step is small enough so that there is no interaction of waves from neighboring Riemann problems. This would be necessary if we wanted to construct the solution at $\mathbf{U}^{n+1}_i$ in order to explicitly calculate the cell average (63). If positivity of all water depth values in the solutions is guaranteed, $h^{**}_i \geq 0$ and $h^*_{i+1} \geq 0$, according to [9], in order to use the flux formula (65) it is only necessary that the edge values $\hat{\mathbf{U}}(x,t)$ remain constant in time over the entire time step, which allows a time step roughly twice as large and the time step is limited by

$$\Delta t \leq \Delta t^{\widetilde{\lambda}} \qquad \Delta t^{\widetilde{\lambda}} = \frac{\Delta x}{\max_{m=1,2}|\widetilde{\lambda}^m|} \tag{69}$$

As the cell average is constructed averaging with the terms $\mathbf{U}^{**}_i$ and $\mathbf{U}^*_{i+1}$, the appearance of negative values of h^{**}_i and h^*_{i+1} must be considered. Figure 12 represents a case with a negative value of h^{**}_{i+1} at a $i+1/2$ edge, where the flow is locally subcritical as in (35). As the approximate solutions used in each RP are independent, it is necessary to

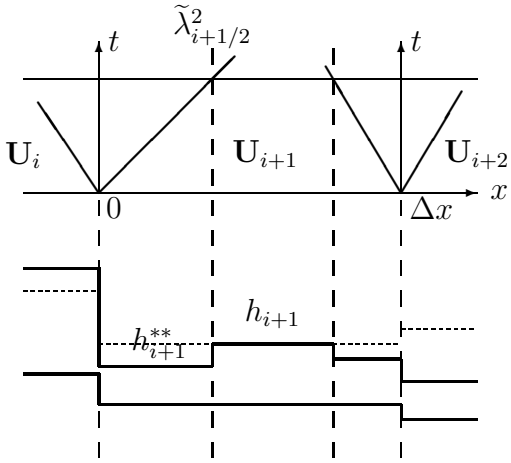

Figure 12: Solution $\hat{\mathbf{U}}(x,t)$.

define the time step ensuring that the cell average value in the control volume $[0, \frac{1}{2}\Delta x]$ remains positive

$$h^{n+1}_{i+1}\frac{1}{2}\Delta x = h^{**}_{i+1}(\widetilde{\lambda}^2_{i+1/2}\Delta t) + h^n_{i+1}(\frac{1}{2}\Delta x - \widetilde{\lambda}^2_{i+1/2})\Delta t \geq 0 \tag{70}$$

leading to the following limit in the size of the time step

$$\Delta t \leq \Delta t^{**} \qquad \Delta t^{**} = \frac{1}{2}\frac{\Delta x}{\widetilde{\lambda}^2_{i+1/2}}\frac{h^n_{i+1}}{h^n_{i+1} - h^{**}_{i+1}} \tag{71}$$

or in the case $h^*_i < 0$

$$\Delta t \leq \Delta t^{*} \qquad \Delta t^{*} = \frac{1}{2}\frac{\Delta x}{\widetilde{\lambda}^1_{i+1/2}}\frac{h^n_{i}}{h^n_{i} - h^{*}_{i}} \tag{72}$$

One case of special interest are wet/dry interfaces with discontinuous bed level, as it is possible to generate negative water depths in the initially dry region of $\hat{\mathbf{U}}(x,t)$. According to (71) or (72) the time step becomes nil in that case. To ensure positivity and conservation of the solution for all cases the Godunov's method is formulated as follows:

$$\mathbf{U}^{n+1}_i = \mathbf{U}^n_i - \left((\delta\mathbf{F} - \mathbf{S})^+_{i-1/2} + (\delta\mathbf{F} - \mathbf{S})^-_{i+1/2}\right)\frac{\Delta t}{\Delta x} \tag{73}$$

where the fluxes in a general intercell edge $i + 1/2$ are computed as follows:

- If $h^n_{i+1} = 0$ and $h^{**}_{i+1} < 0$ set:

$$(\delta\mathbf{F} - \mathbf{S})^-_{i+1/2} = (\delta\mathbf{F} - \mathbf{S})_{i+1/2} \qquad (\delta\mathbf{F} - \mathbf{S})^+_{i+1/2} = 0 \tag{74}$$

- If $h_i^n = 0$ and $h_i^* < 0$ set:

$$(\delta\mathbf{F} - \mathbf{S})^+_{i+1/2} = (\delta\mathbf{F} - \mathbf{S})_{i+1/2} \qquad (\delta\mathbf{F} - \mathbf{S})^-_{i+1/2} = 0 \tag{75}$$

- Otherwise set:

$$(\delta\mathbf{F} - \mathbf{S})^\pm_{i+1/2} = \sum_{m=1}^{N_\lambda} \left(\widetilde{\lambda}^\pm \theta \alpha \widetilde{\mathbf{e}}\right)^m_{i+1/2} \tag{76}$$

with

$$\widetilde{\lambda}^{\pm,m}_{i+1/2} = \frac{1}{2}(\widetilde{\lambda} \pm |\widetilde{\lambda}|) \tag{77}$$

The two main ways of formulating the Godunov type numerical solution for a system are then presented as it was done before for the scalar case. Note that because the numerical source integral cannot, in general, be written as a difference, it is not possible to include it in the numerical flux difference formulation (66). This means that the balance sought between flux derivatives and sources in the numerical flux based scheme can only be achieved locally by balancing non-zero fluxes through the edges of the control volume instead of setting every component to zero as in (73).

When in supercritical conditions values of $h_i^* < 0$ or $h_{i+1}^{**} < 0$ appear, the cell averaging in the Godunov method avoids negative values of h, as the source term does not participate in the updating of the water depth. In consequence, the stability region becomes:

$$\Delta t \leq \begin{cases} \min(\Delta t^{**}, \Delta t^*, \Delta t^{\widetilde{\lambda}}) & \text{if}(\widetilde{\lambda}^1\widetilde{\lambda}^2)_{i+1/2} < 0 \\ \Delta t^{\widetilde{\lambda}} & \text{otherwise} \end{cases} \tag{78}$$

where Δt^{**} is defined as in (71) if $h_{i+1}^{**} < 0$ and $h_{i+1}^n \neq 0$ and Δt^* is defined as in (72) if $h_i^* < 0$ and $h_i^n \neq 0$.

One result of Roe's linearization is that the resulting approximate Riemann solution consists of only discontinuities and $\hat{\mathbf{U}}(x,t)$ is constructed as a sum of jumps or shocks. To avoid unphysical results the version of the Harten-Hyman entropy fix [18] is used. In the case of left transonic rarefaction $\lambda_i^1 < 0 < \lambda_{i+1}^1$, with $\lambda_i = \lambda(\mathbf{U}_i)$ and $\lambda_{i+1} = \lambda(\mathbf{U}_{i+1})$, the jump associated to $\widetilde{\lambda}^1_{i+1/2}$ is decomposed into two new jumps,

$$\bar{\lambda}^1 = \lambda_i^1 \frac{(\lambda_{i+1}^1 - \widetilde{\lambda}^1)}{(\lambda_{i+1}^1 - \lambda_i^1)} \qquad \widehat{\lambda}^1 = \lambda_{i+1}^1 \frac{(\widetilde{\lambda}^1 - \lambda_i^1)}{(\lambda_{i+1}^1 - \lambda_i^1)} \tag{79}$$

with $\bar{\lambda}^1 + \widehat{\lambda}^1 = \widetilde{\lambda}^1$, and $\bar{\lambda}^1 < 0$ and $\widehat{\lambda}^1 > 0$ by definition.

This idea can be applied to the decomposition of the source term associated to β^1 into two new values, $\bar{\beta}^1$ and $\widehat{\beta}^1$. Their definition has to be done enforcing a conservative

splitting of the source terms, $\bar{\beta}^1 + \widehat{\beta}^1 = \beta^1$. Numerically it is possible to force a splitting proportional to the one performed on the $\widetilde{\lambda}^1_{i+1/2}$ wave, that is

$$\bar{\beta}^1 = \beta^1 \frac{\bar{\lambda}^1}{\widetilde{\lambda}^1} \qquad \widehat{\beta}^1 = \beta^1 \frac{\widehat{\lambda}^1}{\widetilde{\lambda}^1} \tag{80}$$

but this option results in erroneous results and in a reduction of the time step size, as the values of $\bar{\beta}^1$ and $\widehat{\beta}^1$ as defined in (80) are much greater than the original one, β^1, as under these conditions $\widetilde{\lambda}^1$ is a travelling wave with almost nil velocity. The option used in this work is

$$\bar{\beta}^1 = \beta^1 \qquad \widehat{\beta}^1 = 0 \tag{81}$$

that preserves the stability region in (78), simply replacing $\widetilde{\lambda}^1_{i+1/2}$ by $\bar{\lambda}^1_{i+1/2}$.

For a right transonic rarefaction $\lambda^2_i < 0 < \lambda^2_{i+1}$, the entropy fix procedure is entirely analogous to the left rarefaction case. The single jump in $\widetilde{\lambda}^2$ is split into two smaller jumps $\bar{\lambda}^2$ and $\widehat{\lambda}^2$

$$\bar{\lambda}^2 = \lambda^2_{i+1} \frac{(\widetilde{\lambda}^2 - \lambda^2_i)}{(\lambda^2_{i+1} - \lambda^2_i)} \qquad \widehat{\lambda}^2 = \lambda^2_i \frac{(\lambda^2_{i+1} - \widetilde{\lambda}^2)}{(\lambda^2_{i+1} - \lambda^2_i)} \tag{82}$$

with $\bar{\lambda}^2 > 0$ and $\widehat{\lambda}^2 < 0$ by definition. The source term is split enforcing

$$\beta^2 = \beta^2 \qquad \bar{\beta}^2 = 0 \tag{83}$$

so the stability region in (78) is preserved, simply replacing $\widetilde{\lambda}^2_{i+1/2}$ by $\bar{\lambda}^2_{i+1/2}$.

3.2 Integration of the source term

The source term in (51) is expressed as

$$\mathbf{S}_{i+1/2} = \begin{pmatrix} 0 \\ \frac{p_b}{\rho_w} - \frac{\tau_b}{\rho_w} \end{pmatrix}_{i+1/2} \tag{84}$$

where $\frac{p_b}{\rho_w}$ and $\frac{\tau_b}{\rho_w}$ attend to the pressure and friction exerted on the bed respectively.

There is not a unique way to perform the numerical integral of the source term in (51). Under the hypothesis of smooth variation of the variables and an infinitesimal width of the control volume, it is possible to define the integral in (51) evaluating $\frac{p_b}{\rho_w}$ as

$$\left(\frac{p_b}{\rho_w} \right)^a_{i+1/2} = -g(\widetilde{h}\delta z)_{i+1/2} \tag{85}$$

with $\widetilde{h} = 1/2(h_i + h_{i+1})$. Assuming a piecewise representation of the bed level, another possibility is to use the physical definition of the hydrostatic force exerted over the bed

discontinuity so the pressure head depends only on the free-surface level. Attending to this definition, (51) is defined using the following approach for $\frac{p_b}{\rho_w}$:

$$\left(\frac{p_b}{\rho_w}\right)^b_{i+1/2} = -g\left(h_j - \frac{|\delta z'|}{2}\right)\delta z' \tag{86}$$

with

$$j = \begin{cases} i & \text{if } \delta z \geq 0 \\ i+1 & \text{if } \delta z < 0 \end{cases} \qquad \delta z' = \begin{cases} h_i & \text{if } \delta z \geq 0 \text{ and } d_i < z_{i+1} \\ h_{i+1} & \text{if } \delta z < 0 \text{ and } d_{i+1} < z_i \\ \delta z & \text{otherwise} \end{cases} \tag{87}$$

where $d = (h + z)$. Both approaches can be blended to provide another expression for the thrust term, that we will refer to as $\left(\frac{p_b}{\rho_w}\right)^c$:

$$\left(\frac{p_b}{\rho_w}\right)^c_{i+1/2} = \begin{cases} \max\left(\left(\frac{p_b}{\rho_w}\right)^a, \left(\frac{p_b}{\rho_w}\right)^b\right)_{i+1/2} & \text{if } \delta d\, \delta z \geq 0 \text{ and } \widetilde{u}\delta z > 0 \\ \left(\frac{p_b}{\rho_w}\right)^b_{i+1/2} & \text{otherwise} \end{cases} \tag{88}$$

that considers the problems associated to flow across an upward step in overtopping waves.

In cases of still water with a continuous water level surface all three approximations of the trust term, a, b and c, provide correct solutions for all values when constructing the approximate solution $\hat{\mathbf{U}}(x,t)$, as in this particular case, Figure 13:

$$\begin{gathered} h_i^n + z_i = h_i^* + z_i = h_{i+1}^{**} + z_{i+1} = h_{i+1}^n + z_{i+1} \\ (hu)_i^n = (hu)_i^* = (hu)_{i+1}^{**} = (hu)_{i+1}^n = 0 \end{gathered} \tag{89}$$

This is a particular case, and in cases of non zero velocity, differences among the solutions provided by the source term integral in $(p_b/\rho_w)^a$, $(p_b/\rho_w)^b$ and $(p_b/\rho_w)^c$ arise. One consequence of utmost importance is that they can generate negative values of water depth in the inner regions of the weak solution. In wetting/drying fronts negative values can be avoided if in each $i+1/2$ edge with discontinuous water level surface, characterized by

$$h_i^n + z_i < z_{i+1}, \qquad h_{i+1}^n = 0 \tag{90}$$

or

$$h_{i+1}^n + z_{i+1} < z_i, \qquad h_i^n = 0 \tag{91}$$

a zero velocity in the involved cells is enforced, $u_{i+1}^n = u_i^n = 0$, in combination with approach $(p_b/\rho_w)^c$. This procedure, that considers the cell edges characterized by (90) or (91) as solid walls, will be referred to as approach $(p_b/\rho_w)^{c,w}$.

Regarding the friction term, the discretization based on [12] is applied

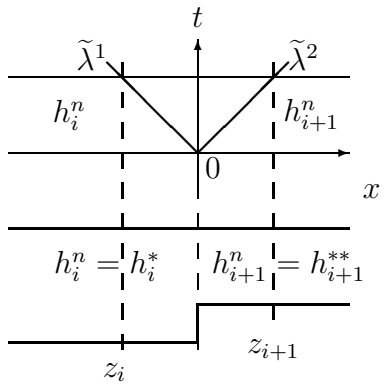

Figure 13: Solution $\hat{\mathbf{U}}(x,t)$ in case of static equilibrium.

$$\frac{\tau_b}{\rho_w}_{f,i+1/2} = g(\widetilde{h}S_f)_{i+1/2}\Delta x \qquad S_{f,i+1/2} = \left(\frac{n^2\widetilde{u}|\widetilde{u}|}{\max(h_i, h_{i+1})^{4/3}}\right)_{i+1/2} \tag{92}$$

The importance of the discrete equilibrium in cases of still water to provide well-balanced schemes has been widely reported, but it is important to stress that with the unified formulation of the source terms, the scheme becomes well balanced in steady cases with no null velocity. According to numerical scheme (73), the stationary solution is reached when all updating components of the linearized solution become nil, that is $(\theta\alpha)^m_{i+1/2} = 0$ for $m = 1, 2$, leading to a constant discharge in all zones of the weak solution. In the subcritical case:

$$(hu)_i^n = (hu)_i^* = (hu)_{i+1}^{**} = (hu)_{i+1}^n \neq 0 \tag{93}$$

or in the supercritical case, with $u > 0$:

$$(hu)_i^n = (hu)_{i+1}^* = (hu)_{i+1}^{**} = (hu)_{i+1}^n \neq 0 \tag{94}$$

3.3 Reconstruction of the approximate solution $\hat{\mathbf{U}}(x,t)$

The linearization of the source terms leads to extremely small values of the allowable time step, as Δt^{**} or Δt^* can be various order of magnitude smaller than $\Delta t^{\widetilde{\lambda}}$. This can be avoided by means of a reconstruction of the approximate solution $\hat{\mathbf{U}}(x,t)$. The strategy proposed here is based on enforcing positive values of h_i^* and h_{i+1}^{**} when they become negative. Considering that $\widetilde{e}_1^1 = 1$, positive values of h_i^* require that

$$h_i^* = h_i^n + \alpha_{i+1/2}^1 - \left(\frac{\beta}{\widetilde{\lambda}}\right)^1_{i+1/2} \geq 0 \tag{95}$$

leading to the following limit over β^1

$$\beta^1_{i+1/2} \geq \beta^1_{min} \qquad \beta^1_{min} = -\left(h^n_i + \alpha^1_{i+1/2}\right) |\widetilde{\lambda}^1_{i+1/2}| \tag{96}$$

Considering that $\widetilde{e}^2_1 = 1$, positive values of h^{**}_{i+1} require that

$$h^{**}_{i+1} = h^n_{i+1} - \alpha^2_{i+1/2} + \left(\frac{\beta}{\widetilde{\lambda}}\right)^2_{i+1/2} \geq 0 \tag{97}$$

and a limit over β^2 appears

$$\beta^2_{i+1/2} \geq \beta^2_{min} \qquad \beta^2_{min} = -\left(h^n_{i+1} - (\alpha)^2_{i+1/2}\right) \widetilde{\lambda}^2_{i+1/2} \tag{98}$$

The reconstruction proposed in this work will be applied only to subcritical wet/wet RP, as in dry/wet RP the appearance of negative values of h^*_i or h^{**}_{i+1} in the approximate solution is helpful to provide a correct tracking of the flooding advance, and in supercritical cases the cell averaging of the weak solutions ensures positivity of the solution. Also cases where both $h^*_i < 0$ and $h^{**}_{i+1} < 0$ are omitted.

In the case $h^*_i < 0$ and $h^{**}_{i+1} > 0$ and $\Delta t^* < \Delta t^{\widetilde{\lambda}}$, the new value of β^1 is redefined ensuring that h^{**}_{i+1} remains positive or null. To ensure conservation β^2 must be replaced by the new value of $-\beta^1$, then

$$\beta^1 = \begin{cases} \beta^1_{min} & \text{if} \quad -\beta^1_{min} \geq \beta^2_{min} \\ \beta^1 & \text{otherwise} \end{cases}, \qquad \beta^2 = -\beta^1 \tag{99}$$

In the case $h^*_i > 0$ and $h^{**}_{i+1} < 0$ and $\Delta t^{**} < \Delta t^{\widetilde{\lambda}}$, the new value of β^2 is redefined ensuring that h^*_i remains positive or null. To ensure conservation β^1 must be replaced by the new value of $-\beta^2$, then

$$\beta^2 = \begin{cases} \beta^2_{min} & \text{if} \quad -\beta^2_{min} \geq \beta^1_{min} \\ \beta^2 & \text{otherwise} \end{cases}, \qquad \beta^1 = -\beta^2 \tag{100}$$

3.4 Dam break test cases.

In this section we present comparisons among exact solutions of the Riemann problem for system (1), neglecting friction, and numerical solutions. The exact solution corresponding to a frictionless dambreak flow over a discontinuous bed is detailed in Appendix C. The results are presented in the form of plots of the total depth, mean discharge, Froude number and energy per unit weight or head. The examples are chosen to represent different combinations of wave patterns. The acceleration due to gravity is set equal to $g = 9.8m^2/s$. In all cases the bottom step is positioned at $x = 0$ and has a variable height. In all cases $\Delta x = 1$ and CFL = 1. When applying the reconstruction technique of the weak solution proposed in (99) and (100) no difference in the solution has been observed when comparing with the original solution.

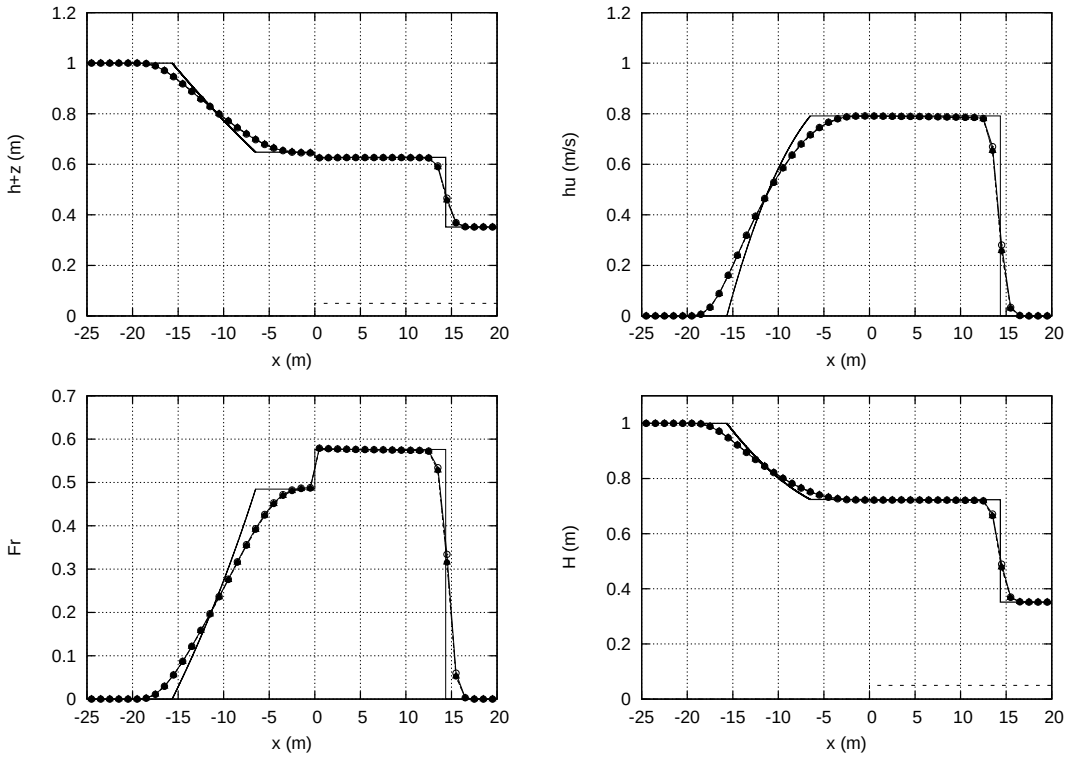

Figure 14: Test case 1: comparison between exact (—) and numerical solutions at t=5s obtained with approaches $(p_b/\rho_w)^a(-\circ-)$, $(p_b/\rho_w)^b(-\bullet-)$, $(p_b/\rho_w)^c(-\triangle-)$

Table 1: Summary of test cases.

Test Case	h_L	h_R	u_L	u_R	z_L	z_R
1	1.0	0.30179953	0.0	0.0	0.0	0.05
2	4.0	0.50537954	0.1	0.0	0.0	1.5
3	2.5	2.49977381	1.5	0.0	0.0	0.25
4	1.5	0.16664757	2.0	0.0	0.0	2.0
5	1.0	0.04112267	0.2	0.0	0.25	0.0
6	0.6	0.02599708	0.35	0.0	1.2	0.0
7	1.1	0.49457729	4.9	6.50	0.2	0.0
8	1.5	0.0	2.2862	0.0	0.0	4.0
9	1.5	0.0	4.5	0.0	0.0	4.0
10	1.5	0.0	-2.5	0.0	0.0	1.0
11	1.5	0.0	-5.0	0.0	0.0	1.0

Test case 1 is a dam-break type problem, with a combination of rarefaction and shock waves. The initial condition consists of two columns of water of different height and zero velocity. The solution, presented in Fig. 14 , contains a left moving rarefaction wave, a stationary shock at the step and a right-moving shock wave. The presence of the step leads to a reduction of the total water height running to the right as compared to the flat bottom case. This reduction is due to the stationary shock, which dissipates part of the energy of the shock wave. All three approximations of the pressure term, $(p_b/\rho_w)^a$,$(p_b/\rho_w)^b$ and $(p_b/\rho_w)^c$, provide results of similar accuracy, for the total depth, mean velocity, Froude number and energy. The options $(p_b/\rho_w)^b$ and $(p_b/\rho_w)^c$ in particular overlap completely so that they cannot be distinguished in the plot. The position of the fan expansion and the shock are correct and the discharge does not present oscillations in the origin. The correct behavior of the numerical scheme is explained attending to the characteristics of the weak solution, that in a subcritical case, provides a constant value of discharge for the two inner regions $\mathbf{U}_i^*$ and $\mathbf{U}_{i+1}^{**}$, according to the exact solution.

Test case 2 is also a dam-break type problem, with a combination of rarefaction and shock waves. The initial condition consists of two columns of water of different heights and velocity on the left side. The solution, presented in Fig. 15, contains a left moving rarefaction wave, a stationary shock at the step and a right-moving shock wave. The numerical solution for approximation $(p_b/\rho_w)^a$ differs strongly from the analytical solution for all the plotted variables, and also provides an increment of the total water height. Approximations of the pressure term, $(p_b/\rho_w)^b$ and $(p_b/\rho_w)^c$, provide the same results, leading to a correct description of the total depth, the mean discharge, Froude number and compute the energy dissipation correctly.

Test case 3 is a two shock case with a convergent flow. The solution is presented in Figure 16, and contains a left-moving shock, a stationary shock at the step and a right-moving shock wave. As in the previous example, the step acts as an energy dis-

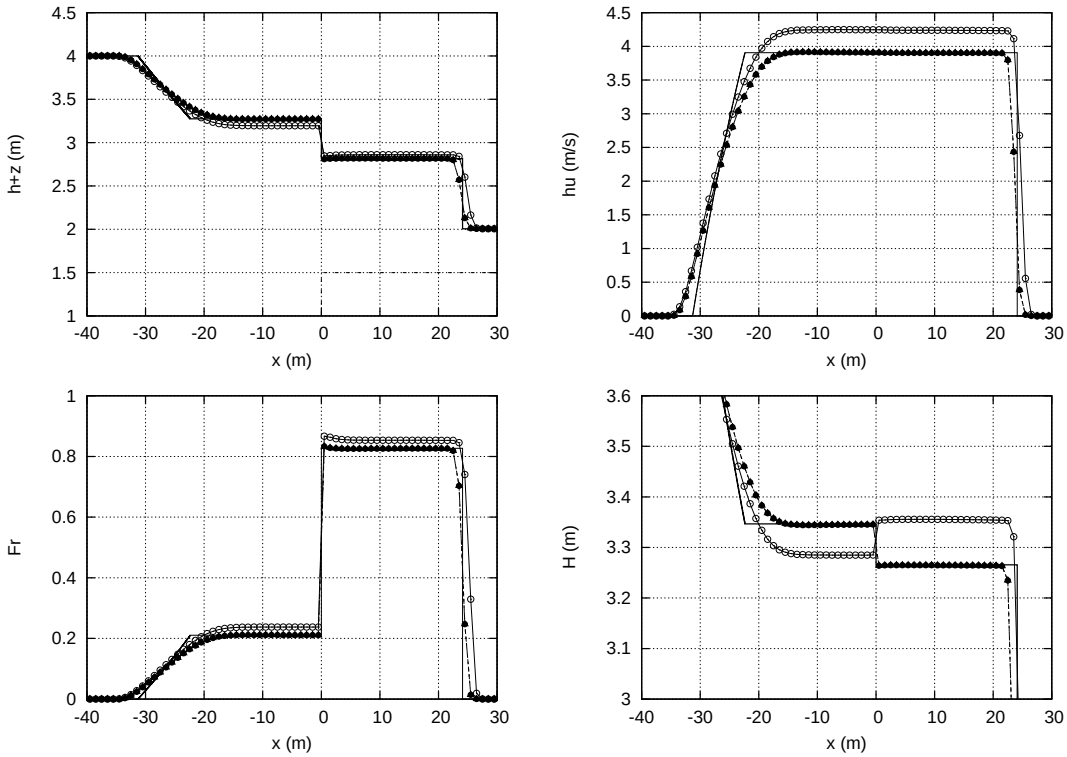

Figure 15: Test case 2: comparison between exact (—) and numerical solutions at t=5s obtained with approaches $(p_b/\rho_w)^a(-\circ-)$, $(p_b/\rho_w)^b(-\bullet-)$, $(p_b/\rho_w)^c(-\triangle-)$

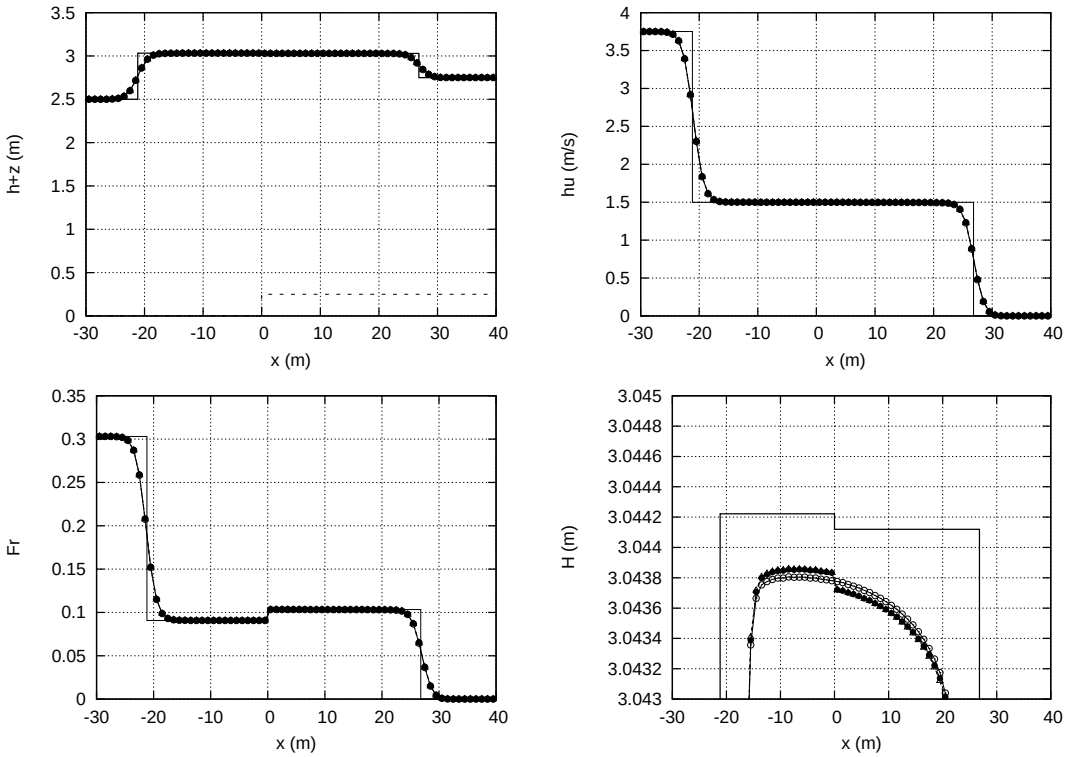

Figure 16: Test case 3: comparison between exact (——) and numerical solutions at t=5s obtained with approaches $(p_b/\rho_w)^a(-\circ-)$, $(p_b/\rho_w)^b(-\bullet-)$, $(p_b/\rho_w)^c(-\triangle-)$

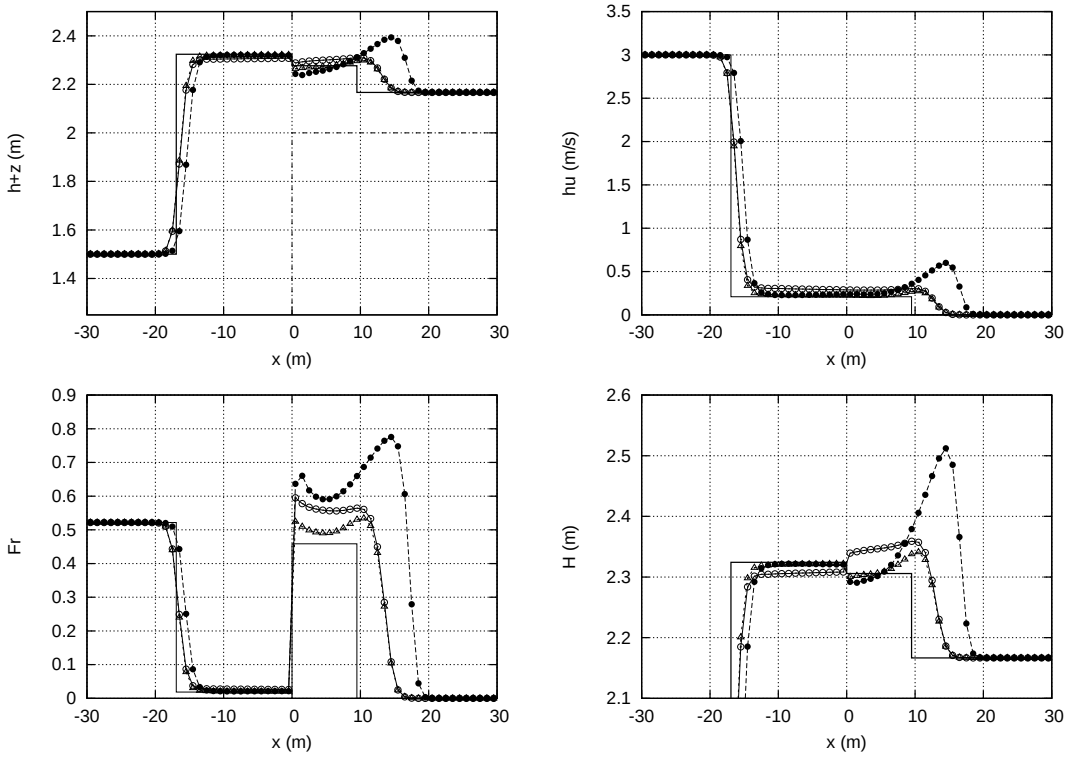

Figure 17: Test case 4: comparison between exact (——) and numerical solutions at t=5s obtained with approaches $(p_b/\rho_w)^a(-\circ-)$, $(p_b/\rho_w)^b(-\bullet-)$, $(p_b/\rho_w)^c(-\triangle-)$

sipation mechanism. All three approximations of the pressure term, $(p_b/\rho_w)^a$,$(p_b/\rho_w)^b$ and $(p_b/\rho_w)^c$, provide results of similar accuracy, for the total depth, mean discharge and Froude number, as this case corresponds to a relatively mild slope. The strongest differences appear in the total water height, with $(p_b/\rho_w)^b$ and $(p_b/\rho_w)^c$ providing the most energy dissipative solutions.

Test case 4 is also a two shock case with a convergent flow, with an initial discontinuity in the water depth. The performance of the numerical scheme in cases with this type of discontinuity is of major importance in practice. As in test case 3, the solution, depicted in Figure 17, contains a left-moving shock, a stationary shock at the step and a right-moving shock wave. All solutions provide an adequate description of the water discharge at the dam break position, $x = 0m$, but the differences among the results for the rest of variables are noticeable. Approach $(p_b/\rho_w)^a$ lead to unphysical result for the total water height, while approach $(p_b/\rho_w)^b$, strongly overestimates the velocity of the right moving shock and underestimates the velocity of the left moving shock. The hybrid option $(p_b/\rho_w)^c$ combines the best properties of both approaches leading to superior results, not only providing an energy dissipating solution but also reaching better results for the rest of variables. The differences with the exact solution are attributable to the linearization of the source term when constructing the weak solution.

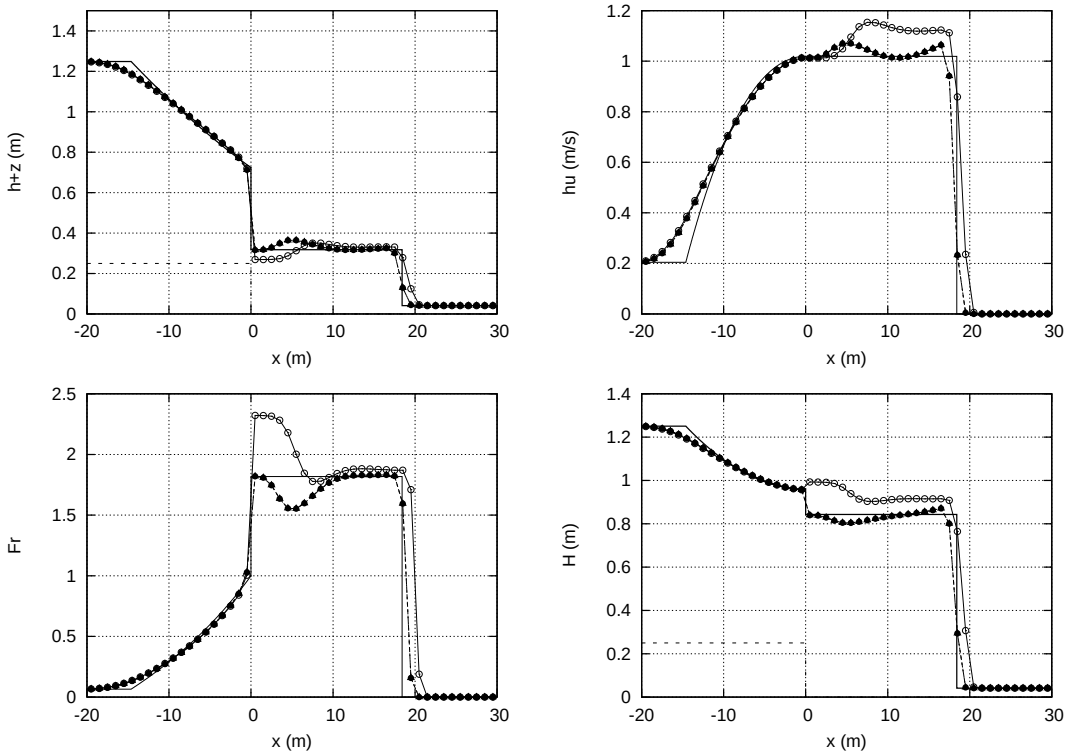

Figure 18: Test case 5: comparison between exact (—) and numerical solutions at t=5s obtained with approaches $(p_b/\rho_w)^a(-\circ-)$, $(p_b/\rho_w)^b(-\bullet-)$, $(p_b/\rho_w)^c(-\triangle-)$

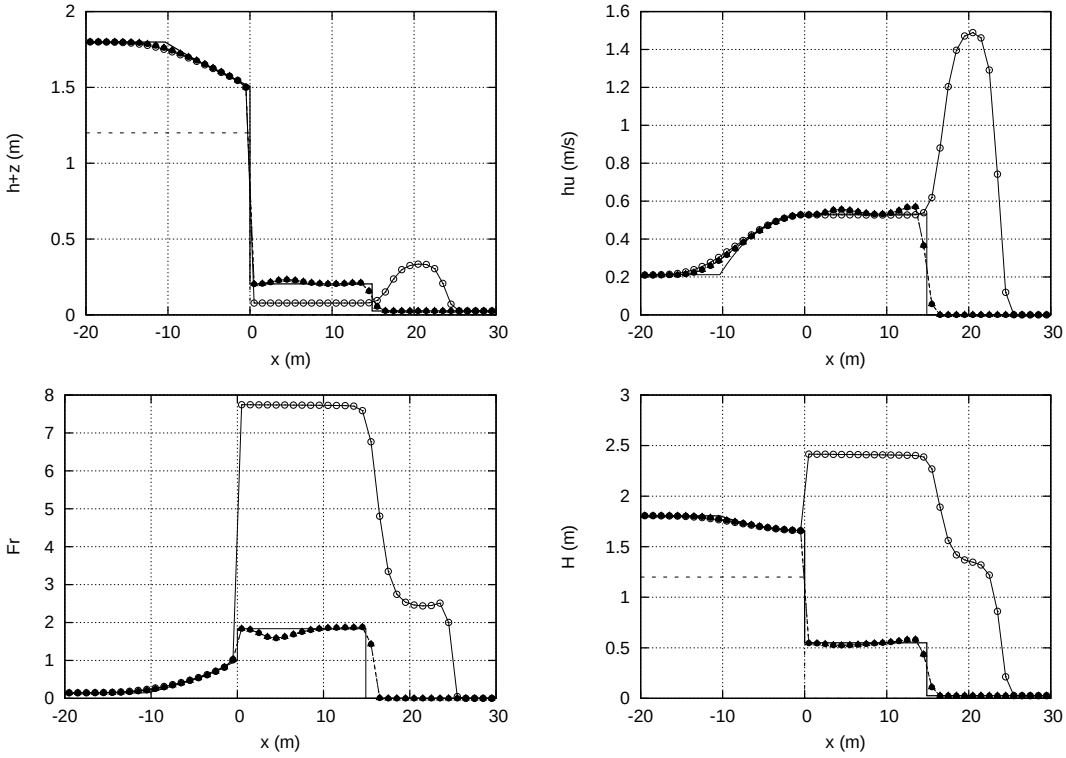

Figure 19: Test case 6: comparison between exact (——) and numerical solutions at t=5s obtained with approaches $(p_b/\rho_w)^a(-\circ-)$, $(p_b/\rho_w)^b(-\bullet-)$, $(p_b/\rho_w)^c(-\triangle-)$

Test case 5 is a dam-break type problem, with a combination of rarefaction and shock waves, but in contrast with test cases 1 and 2, the initial condition consists of two columns of water of different heights, velocity in the left side and a backward step of height similar to the right column of water. The solution, presented in Fig. 18, contains a left moving rarefaction wave, a stationary shock at the step and a right-moving shock wave. The presence of the step dissipates part of the energy. Approximations of the pressure term $(p_b/\rho_w)^b$ and $(p_b/\rho_w)^c$, that provide identical results, lead to a description of the total depth, the mean discharge, Froude number and compute the energy dissipation closer to the exact solution. Again, the differences still shown by approaches $(p_b/\rho_w)^b$ and $(p_b/\rho_w)^c$ with respect to the exact solution are attributable to the linearization of the source term when constructing the weak solution. Test case 6 is similar to test case 5, but with a stronger discontinuity in the water elevation, and a very thin layer of water 0n the right side. The solution is presented in Fig. 19. Only approximations of the pressure term $(p_b/\rho_w)^b$ and $(p_b/\rho_w)^c$, that provide identical results, lead to a correct description of the total depth, the mean discharge, Froude number and compute the energy dissipation. Approach $(p_b/\rho_w)^a$, provides a solution totally inadequate and distorted if compared with the analytical case.

In test case 7 a supercritical motion from left to right is considered. The presence

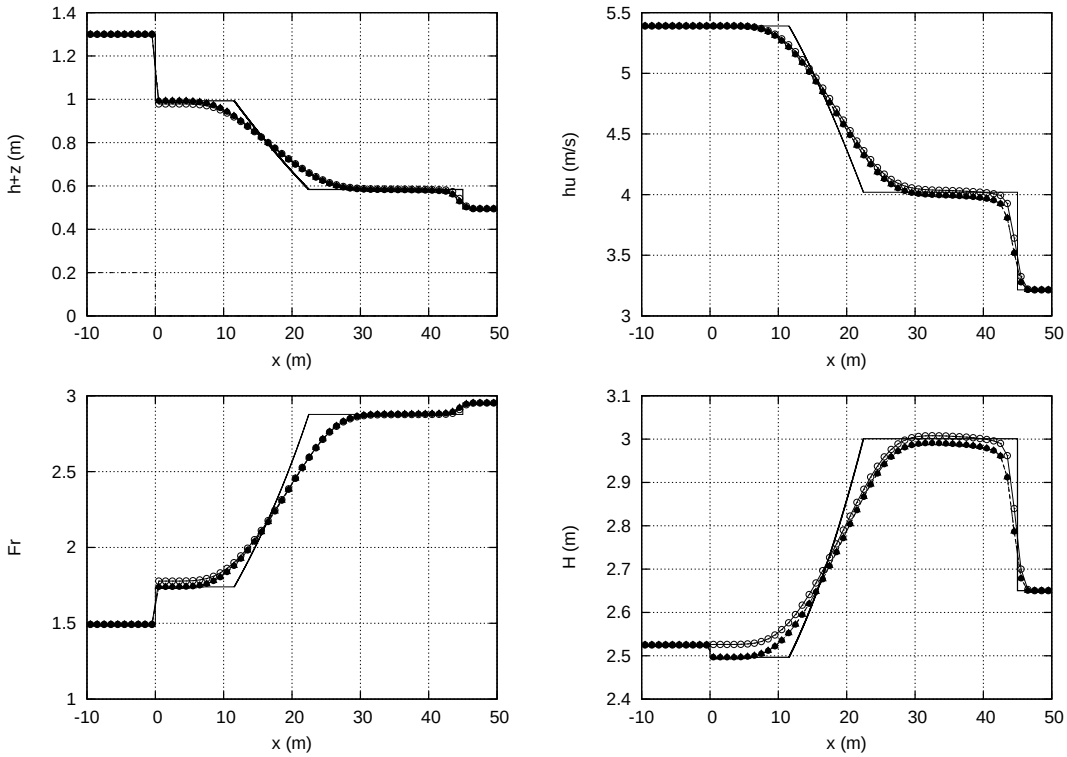

Figure 20: Test case 7: comparison between exact (—) and numerical solutions at t=5s obtained with approaches $(p_b/\rho_w)^a(-\circ-)$, $(p_b/\rho_w)^b(-\bullet-)$, $(p_b/\rho_w)^c(-\triangle-)$

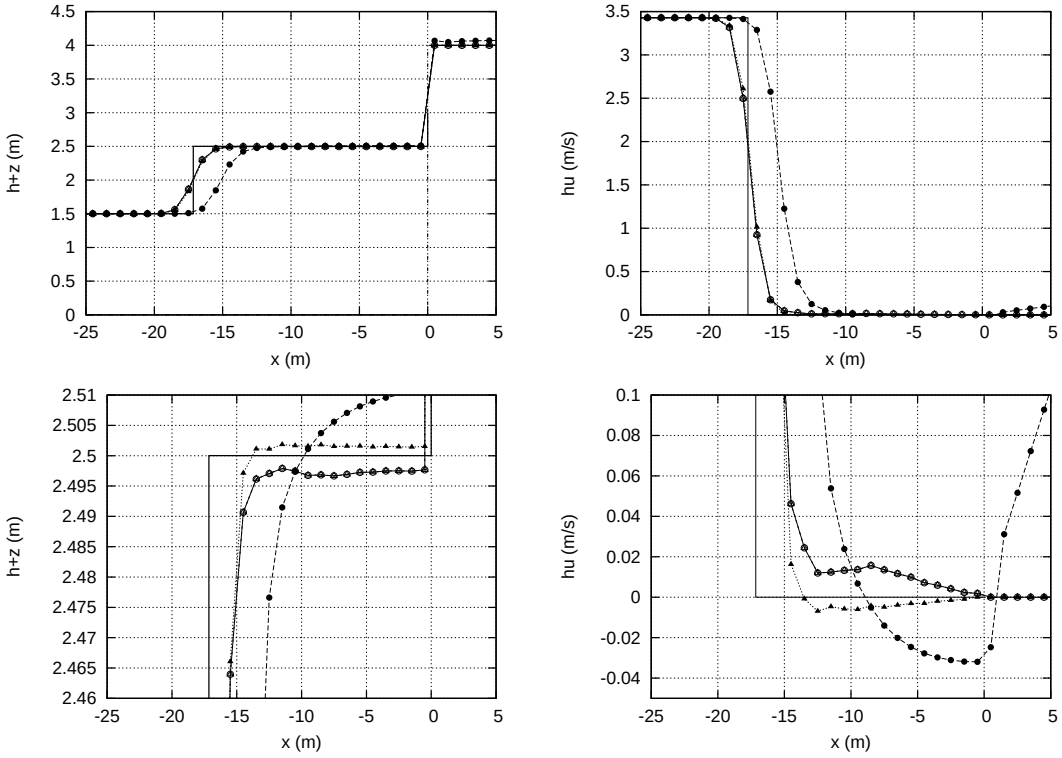

Figure 21: Test case 8: comparison between exact (——) and numerical solutions at t=5s obtained with approaches $(p_b/\rho_w)^a(-\circ-)$, $(p_b/\rho_w)^b(-\bullet-)$, $(p_b/\rho_w)^c(-\triangle-)$, $(p_b/\rho_w)^{c,w}(--)$

of the step introduces no limitation in the signal propagation upstream, and its effect is in dissipating energy by the stationary shock at the step. The solution, presented in Fig. 20, contains a stationary shock at the step, a right moving rarefaction wave, and a right-moving shock wave. Only approximations of the pressure term $(p_b/\rho_w)^b$ and $(p_b/\rho_w)^c$, that provide identical results, lead to a correct description of the total depth, the mean discharge, Froude number and compute the energy dissipation correctly. Approach $(p_b/\rho_w)^a$, provides an unphysical solution for the total water height. For all approaches the computed discharge is kept constant and equal to the left value, $(hu)_L$, until the solution reaches the rarefaction wave. This is explained attending to the definition of the weak solution for supercritical cases in (**??**), that provides an adequate value for the inner region, resulting in $(hu)_i^n = (hu)_{i+1}^*$ according to the exact solution.

In test cases 8 to 11 the performance of the numerical scheme in RPs characterized by a fixed in time wet/dry position are analysed. Depending on the approach of the source term the flow develops in both regions of the plain. This is avoided if the weak solution provides null or negative values of water depth in the initially dry side of the RP. In this context, the performance of the energy dissipative approach $(p_b/\rho_w)^{c,w}$ is of interest.

In test case 8 a subcritical flow encounters a wall and is reflected. The solution, presented in Fig. 21, contains a left-moving shock that links the right moving water with

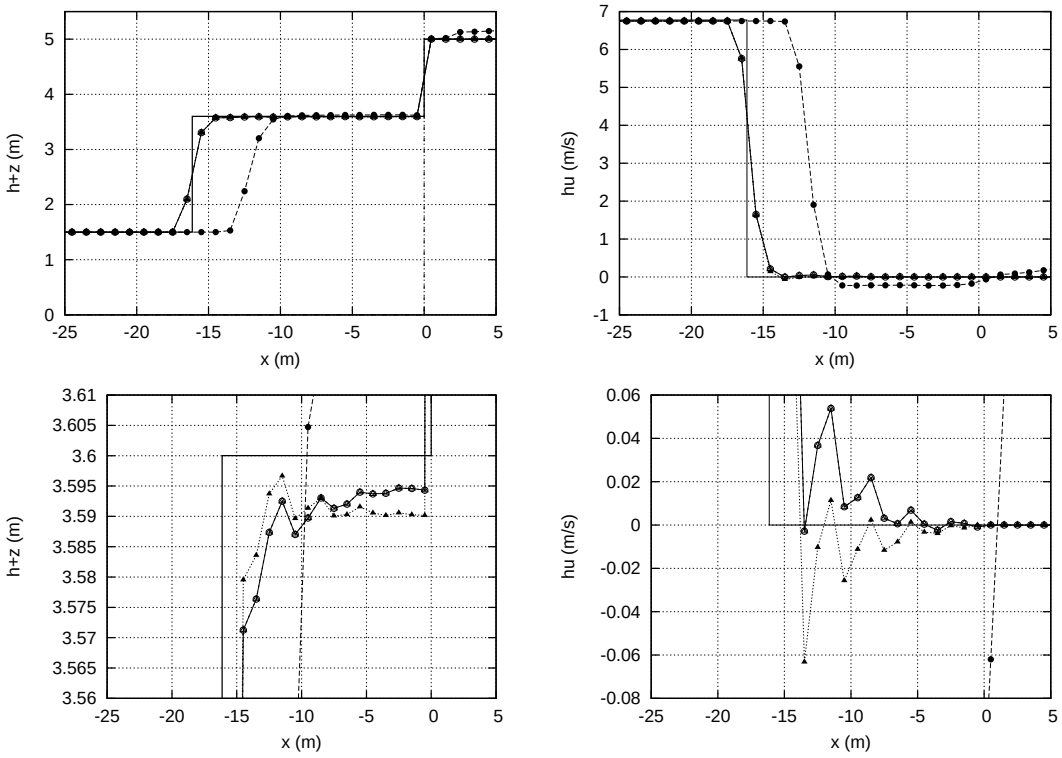

Figure 22: Test case 9: comparison between exact (——) and numerical solutions at t=5s obtained with approaches $(p_b/\rho_w)^a(-\circ-)$, $(p_b/\rho_w)^b(-\bullet-)$, $(p_b/\rho_w)^c(-\triangle-)$, $(p_b/\rho_w)^{c,w}(--)$

a region of still water ending at the stationary shock at $x = 0$. The bed elevation on the right side is greater than the maximum allowable water depth in the wet region at rest. Only approximations of the pressure term $(p_b/\rho_w)^a$, $(p_b/\rho_w)^c$ and $(p_b/\rho_w)^{c,w}$ provide a correct solution in the left side, while $(p_b/\rho_w)^b$, develops in both sides leading to incorrect solutions. Option $(p_b/\rho_w)^{c,w}$ provides more accurate results for both water depth and flow discharge. The same results are observed for test case 9, Fig. 22, where a supercritical flow encounters a wall and is reflected.

In test case 10 a subcritical flow moving to the left generates a left moving rarefaction connecting the left state with a state of water at rest, with a water depth smaller than the depth of the wall defined in the other side. The solution is presented in Fig.23. Approximations of the pressure term $(p_b/\rho_w)^a$ and $(p_b/\rho_w)^c$ develop correctly in the left side of the (x, t) plane, although present an oscillatory behavior in the zero velocity region. The results for approach $(p_b/\rho_w)^{c,w}$ do not present any oscillation in the region of zero velocity but estimate less accurately the velocities at the tail and the head of the rarefaction. Again $(p_b/\rho_w)^b$ provides an incorrect solution.

The situation is much more interesting in test case 11, where supercritical flow conditions are enforced in the left side. Again $(p_b/\rho_w)^b$ provides an incorrect solution and $(p_b/\rho_w)^a$, $(p_b/\rho_w)^c$ lead to similar results. Results given by approach $(p_b/\rho_w)^{c,w}$ follow the

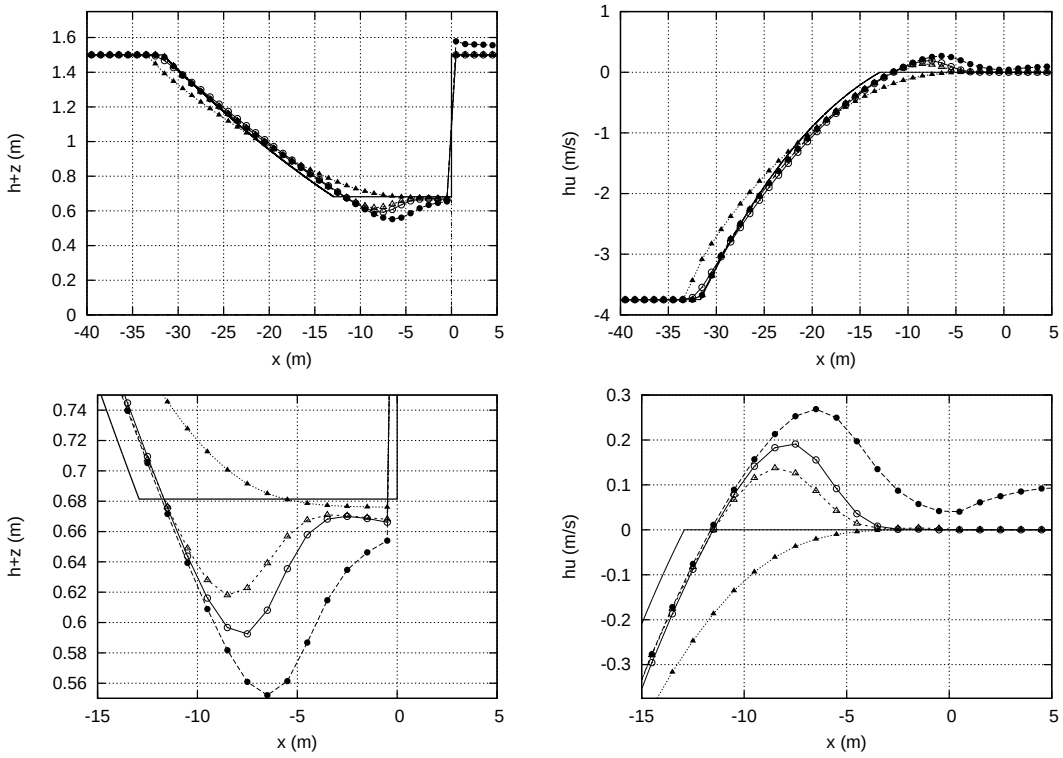

Figure 23: Test case 10: comparison between exact (——) and numerical solutions at t=5s obtained with approaches $(p_b/\rho_w)^a(-\circ-)$, $(p_b/\rho_w)^b(-\bullet-)$, $(p_b/\rho_w)^c(-\triangle-)$, $(p_b/\rho_w)^{c,w}(--)$

same tendency as in test case 10.

According to the hypothesis assumed to derive the exact solution, the solutions in test cases 8 to 11 should be independent of the actual height of the dry step z_R. That is, if the value of the dry bed level z_R decreases until a value equal to the water depth in the region of zero velocity, that will be referred to as $h_{L,0}$, the solution remains equal. However, due to the approximation used to define the bed discontinuity, this has an influence, and before z_R reaches the limit $h_{L,0}$, numerical solutions evolve in both regions. Table 2 shows the numerical limits that can be reached by the value of z_R before the solution is altered. For test cases 8 and 9, among the approaches described, $(p_b/\rho_w)^{c,w}$ provides the most accurate limiting value, denoted $z_R^{c,w}$, while approaches $(p_b/\rho_w)^a$ and $(p_b/\rho_w)^c$ require larger values to ensure a correct solution. If $(p_b/\rho_w)^b$ is used, the solution fails for all values of z_R^b. For test case 10 in Table 2 shows that $(p_b/\rho_w)^{c,w}$ leads to the best results when decreasing the value for z_R and that $(p_b/\rho_w)^b$ fails in all cases. It is noticeable that, in case 11, approaches $(p_b/\rho_w)^a$, $(p_b/\rho_w)^c$ and $(p_b/\rho_w)^{c,w}$ lead to similar limits for z_R.

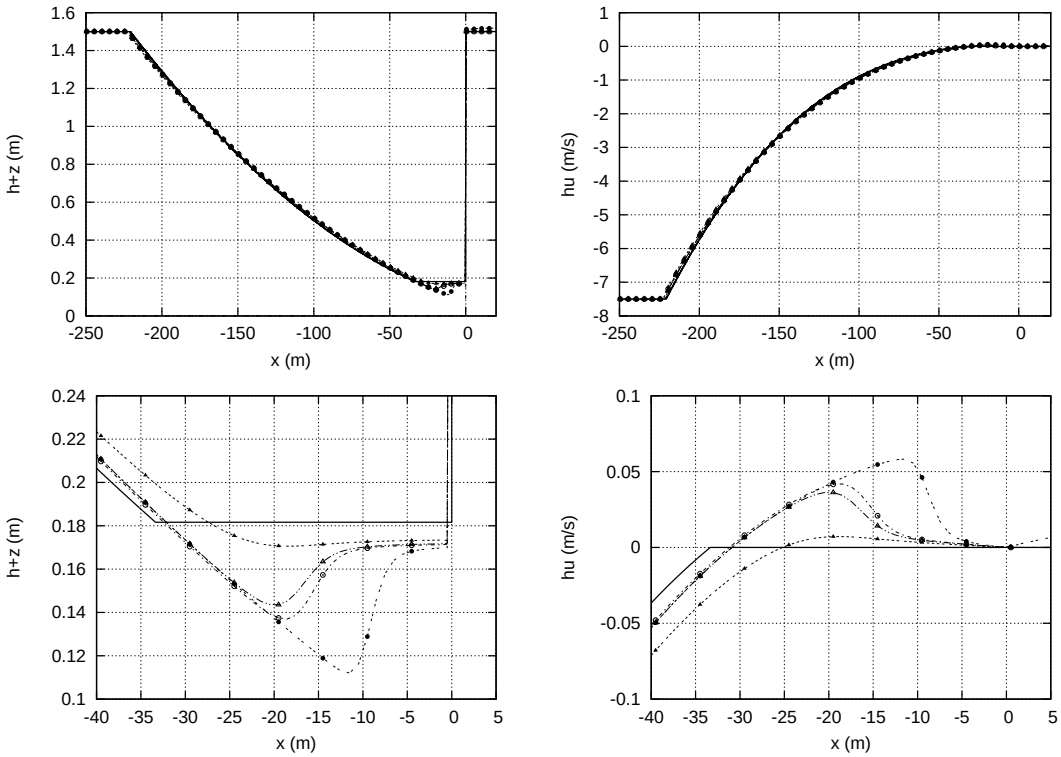

Figure 24: Test case 11: comparison between exact (——) and numerical solutions at t=25s obtained with approaches $(p_b/\rho_w)^a(-\circ-)$, $(p_b/\rho_w)^b(-\bullet-)$, $(p_b/\rho_w)^c(-\triangle-)$, $(p_b/\rho_w)^{c,w}(--)$

Table 2: Numerical limits for z_R.

Test Case	$h_{L,0}$	z_R^a	z_R^b	z_R^c	$z_R^{c,w}$
8	2.50000452	3.2	—	3.2	2.51
9	3.60001180	4.7	—	4.7	3.61
10	0.68136277	0.8	—	0.8	0.68
11	0.18160310	0.18	—	0.18	0.18

4 CONCLUSIONS

In this paper new approximate Riemann solvers problems for systems with source terms have been presented by adding one extra wave associated to the source term. The approximate solution is assumed discontinuous in $x = 0$ and therefore the flux cannot be correctly evaluated assuming the existence of a single value at that location. The method is specifically designed to satisfy the integral formulation.

These wave solutions have been used to rebuild Roe's solver for the discretization of equations with source terms interpreted as non-conservative equations. The approach is based on the wave propagation algorithm in which waves arising in Riemann solutions are directly re-averaged onto adjacent cells in order to update the numerical solution. The method is applicable to both equations in the form of a conservation law as well as those where there is not a flux function (non-conservative equations). The careful procedure of wave averaging in the adjacent cells is the only way to control the stability region of the resulting method as well as the positivity of the variables in all kind of flow conditions. This is the starting point to explore different approximations to the integral source terms in the search for the best properties in each case.

The discretisation proposed is different from the work of many previous authors, who approximated their source terms in a manner which took into account the flux discretisation and, as a consequence, allowed the numerical model to maintain specific equilibria. Previous work dealing with the shallow water system has devoted particular attention to the special case of still water, and the schemes have been constructed so that they maintain this state. In this work, the emphasis is put on a more general idea that is based in the knowledge of non-trivial exact solutions. In fact, the improved accuracy of the new upwind discretisation of the source terms is shown in the approximation of other unsteady exact solutions, particularly in one dimension. Three approaches are discussed for the integral source term, all of them able to fit the trivial quiescent water steady state but different in other cases.

Different methods of integrating source terms, which all respect the classical C-property for water at rest, have been shown to provide different behaviour in specifiec configurations when the water velocity is not equal to zero. Only one of them is recommended as it represents the best compromise in all kind of flows.

The work proposes two modifications over the original Roe's scheme: First, a reformu-

lation of the stability condition that generalizes the classical CFL condition by including the influence of the source terms and the initial conditions in order to avoid the appearance of negative water depth values. Second, a redefinition of the numerical scheme in some particular cases in order to further prevent negative water depth values with independence of the time step. These modifications lead certainly to a considerable CPU time increase in complicated cases. It must be stressed, however, that the modifications are proposed precisely to make the basic method able to cope with complicated cases.

The careful design of the numerical scheme for the equations with source terms requires severe restriction of the allowable time step compatible with numerical stability and positivity in some cases. It is possible to avoid this by limiting the amount of numerical source term involved instead of limiting the time step and leading to more efficient computations. This part does not increase the CPU time but, on the contrary, is included to reduce it. It has been shown that, in combination with the source term approximation, the method produces accurate solutions for a wide variety of time-dependent test cases.

5 ACKNOWLEDGEMENT

This work has been partially funded by the Spanish Ministry of Science and Technology under research project CGL2008-05153-C02-02.

REFERENCES

[1] A.A. Akanbi and N.D. Katopodes. Model for flood propagation on initially dry land. *J. of Hydraulic Engineering* **114**, 689–706, 1987.

[2] F. Alcrudo, F. Benkhaldoun. Exact solutions to the Riemann problem of the shallow water equations with a bottom step. *Comput. Fluids* **30**, 643671, 2001.

[3] R. Bernetti, V.A. Titarev, E.F. Toro. Exact solution of the Riemann problem for the shallow water equations with discontinuous bottom geometry. *Journal of Computational Physics* **227**, 3212–3243, 2008.

[4] P. Brufau, M.E. Vázquez-Cendón and P. García-Navarro. A numerical model for the flooding and drying of irregular domains.*Journal of Numerical Methods in Fluids* **39**, 247–275, 2002.

[5] J. Burguete and P. García-Navarro. Efficient construction of high-resolution TVD conservative schemes for equations with source terms: application to shallow water flows. *International Journal for Numerical Methods in Fluids* **37,**, 209–248, 2001.

[6] R. Courant, E. Isaacson and M. Rees. On the Solution of Nonlinear Hyperbolic Differential Equations by Finite Differences. *Comm. Pure and Appl. Maths.* **5**, 243–255, 1952.

[7] D.L. George. Augmented Riemann solvers for the shallow water equations over variable topography with steady states and inundation. *Journal of Computational Physics* **227**, 3089–3113, 2008.

[8] M. E. Hubbard and P. García-Navarro. Flux difference splitting and the balancing of source terms and flux gradients. *Journal of Comp. Physics* **165**, 89–125, 2000.

[9] R.J. Leveque. *Finite Volume Methods fot Hyperbolic Problems*. Cambridge University Press, New York, 2002, p. 311, 2002.

[10] Q.H. Liang, F. Marche. Numerical resolution of well-balanced shallow water equations with complex source terms. *Advances in water resources* **32**, 873–884, 2009.

[11] J. Murillo, J. Burguete, P. Brufau, and P. García-Navarro. The influence of source terms on stability, accuracy and conservation in two-dimensional shallow flow simulation using triangular finite volumes. *International Journal of Numerical Methods in Fluids* **54**, 543–590, 2007.

[12] J. Murillo, P. García-Navarro and J. Burguete. Time Step Restrictions For Well Balanced Shallow Water Solutions In Non-Zero Velocity Steady States. *International Journal of Numerical Methods in Fluids* **56**, 661–686, 2008.

[13] J. Murillo, P. García-Navarro and J. Burguete. Conservative Numerical Simulation of Multicomponent Transport in Two-Dimensional Unsteady Shallow Water Flo, *Journal of Computational Physics*, **228**, 5539–5573,2009

[14] J. Murillo and P. Garcia-Navarro. Weak solutions for partial differential equations with source terms: Application to the shallow water equations, *Journal of Computational Physics*, **229**, 4327–4368, 2010.

[15] P.L. Roe. *A basis for Upwind Differencing of the Two-Dimensional Unsteady Euler Equations*. Numerical Methods in Fluid Dynamics, Vol II. Oxford University Press, Oxford, 1986.

[16] B.D. Rogers, A.G.L. Borthwick, P.H. Taylor. Mathematical balancing of flux gradient and source terms prior to using Roes approximate Riemann solver. *Journal of Computational Physics* **168**, 422–451, 2003.

[17] G. Rosatti, J. Murillo, L. Fraccarollo. Generalized Roe schemes for 1D two-phase, free-surface flows over a mobile bed. *Journal of Computational Physics* **54**, 543–590, 2007.

[18] W.C. Thacker. Some exact solutions to the non linear shallow water equations. *Journal of Fluid Mechanics* **107**, 499-508, 1981.

[19] E.F. Toro. *Riemann solvers and numerical methods for fluid dynamics*. Springer, Berlin, 1997, p. 526, 1997.

[20] E.F. Toro. *Shock-Capturing Methods for Free-Surface Shallow Flows*. Wiley, New York, 2001, p. 109, 2001.

[21] M.E. Vázquez-Cendón. Improved treatment of source terms in upwind schemes for the shallow water equations in channels with irregular geometry. *Journal of Computational Physics* **148**, 497–498, 1999.

[22] J.G. Zhou, D.M. Causon, C.G. Mingham, D.M. Ingram . The Surface Gradient Method for the Treatment of Source Terms in the Shallow-Water Equations. *Journal of Computational Physics* **168**, 1–25, 2001.